

THE STRESSES PRODUCED BY A SCREW DISLOCATION PILEUP
AT A CIRCULAR INCLUSION OF FINITE RIGIDITY

By

D. Barnett and A. S. Tetelman

Department of Materials Science
Stanford University
Stanford, California

August, 1966

Technical Report # 4

Prepared for the National Aeronautics and Space Administration
Under NASA Contract NSG-622

This paper will appear in the Proceedings of the Conference on Deformation
of Crystalline Solids held in Ottawa, Canada, August 22-26, 1966

1. INTRODUCTION

Dispersed second phase particles and non-metallic inclusions exert a large influence upon the mechanical properties of materials. In addition to increasing the yield strength by raising the stress necessary to move dislocations through the matrix, the presence of dispersed phases and inclusions affects the fracture behavior of these materials by providing sites for void formation via particle or particle-interface cracking at the tip of a blocked slip band. Under applied stresses these voids grow and coalesce, causing fracture at large plastic strains.

Any detailed analysis of the mechanical properties of real materials must therefore include a study of the interactions between slip bands (and cracks) and hard particles, since these interactions play an important role in determining strength and ductility. To a first approximation the slip band-particle interaction may be represented by a planar array of dislocations which has been blocked by, and thus piled up against, the particle (Figure 1).

Before one can investigate the interesting problems of particle fracture, particle-interface fracture, or cross-slip of the piled up dislocations over the barrier, one must first determine the stress distribution associated with such blocked arrays of dislocations as a function of particle shape, size, and rigidity. An analytical treatment of this problem requires, in turn, the selection of an inhomogeneity shape which allows a mathematical solution to be obtained and

THE STRESSES PRODUCED BY A SCREW DISLOCATION PILEUP
AT A CIRCULAR INCLUSION OF FINITE RIGIDITY

By D. M. Barnett⁺ and A. S. Tetelman⁺

ABSTRACT

10887

The method of continuously distributed dislocations is used to obtain the exact solution for the distribution of screw dislocations in a linear array of length L piled up against a circular inclusion of radius R and finite shear modulus. The solution presented is valid for $0 < G_2/G_1 < \infty$, where G_2 is the shear modulus of the inclusion and G_1 is the matrix shear modulus.

The solution enables one to study simultaneously the effects of second phase size and rigidity upon N , the number of dislocations in the pileup, and upon the local stresses induced in the second phase. In the second phase close to the pileup tip it is shown that the local stresses vary as:

- (1) $(2L/\rho)^g$, when the inclusion diameter is much greater than the slip line length
- (2) $\sqrt{\frac{L}{4R}} \left(\frac{4R}{\rho}\right)^g$, when the particle diameter is much less than the slip line length.

ρ is the radial distance from the pileup tip, and g is a function only of the shear moduli ratio, G_2/G_1 , with $0 < g < 1$. The effects of varying second phase size and rigidity upon the magnitude of the local stresses is explained in terms of image dislocation forces generated by the presence of the inhomogeneity ahead of the pileup. *Author*

⁺Department of Materials Science
Stanford University
Stanford, California.

is at the same time a reasonable physical choice. Having chosen the shape, the effect of the remaining variables, size and rigidity (elastic constants), can then be examined. This examination is the subject of the present investigation.

Previous analytical treatments of pileup problems have not simultaneously examined second phase size and rigidity effects upon the induced stress concentrations. A brief summary of these previous treatments and their calculated local stresses is as follows (see also Figure 1):

1. A screw or edge dislocation pileup in an infinite, homogeneous elastic medium (Eshelby, Frank, and Nabarro,⁽¹⁾ 1951). The leading dislocation was assumed to be locked in position by a very short range delta function type force. A similar problem was also studied by Stroh⁽²⁾ in 1954. These problems were analyzed without using the approximation of continuously distributed dislocations.⁽³⁾ Instead, the dislocations in the array were treated as being discrete, and their equilibrium positions were found by the transformation technique of Stieltjes. Close to the pileup tip the local stresses are of the form

$$\tau_{ij} \sim \tau \sqrt{\frac{L}{\rho}} \quad , \quad \left(\frac{L}{\rho} \gg 1\right)$$

where τ is the applied stress, L the pileup length, and ρ the radial distance from the pileup tip. Thus, the local stresses are of the same form as those predicted by continuum fracture mechanics,

$$K = \tau \sqrt{\pi L} ,$$

where K is the stress intensity factor associated with a crack of length L .

2. Head⁽⁴⁾ 1953, provided solutions for single edge and screw dislocations in a bimetallic medium formed by joining two dissimilar elastic half-planes.
3. Chou⁽⁵⁾ 1965, using the single dislocation solution of Head,⁽⁴⁾ considered the screw dislocation pileup against a rigid semi-infinite second phase. This problem and the pileup problems mentioned below were treated by the method of continuously distributed dislocations. It was later shown⁽⁸⁾ that near the pileup tip the local stresses were given by

$$\begin{aligned} \tau_{xz} &\sim \tau \ln \frac{2L}{\rho} \\ \tau_{yz} &\sim \tau \left(\ln \frac{2L}{\rho} \right)^2 . \end{aligned}$$

4. Dundurs⁽⁶⁾ and Dundurs and Mura⁽⁷⁾ in 1965 provided the solutions for single edge and screw dislocations in a matrix containing a circular inclusion.
5. Using the single screw solution given by Dundurs,⁽⁶⁾ Barnett and Tetelman⁽⁸⁾ treated the screw pileup against a rigid circular inclusion of radius R . This represents the introduction of particle size as a free variable. Near the pileup tip

$$\tau_{xz} \sim \tau \ln \frac{2L}{\rho}, \quad \left(\frac{L}{R} \ll 2\right)$$

$$\sim \tau \sqrt{\frac{L}{R}} \ln \frac{4R}{\rho}, \quad \left(\frac{L}{R} \gg 2\right)$$

$$\tau_{yz} \sim \tau \left(\ln \frac{2L}{\rho}\right)^2, \quad \left(\frac{L}{R} \ll 2\right)$$

$$\sim \tau \sqrt{\frac{L}{R}} \left(\ln \frac{4R}{\rho}\right)^2, \quad \left(\frac{L}{R} \gg 2\right).$$

6. A screw pileup against a semi-infinite second phase of finite shear modulus (Barnett,⁽⁹⁾ 1966). Here the condition of finite inclusion size was relaxed and replaced by the introduction of finite rigidity. The pileup was allowed to exist in either the hard or soft phase and the local stresses were found to be of the form

$$\tau_{ij} \sim \tau \left(\frac{2L}{\rho}\right)^g,$$

where g is a function of the ratio of the shear moduli of the respective phases with $0 < g < 1$.

The different expressions for local stress intensification are due to image dislocation forces introduced by the presence of the inhomogeneity. Inclusion size determines the distribution of these image forces, whereas inclusion rigidity determines the strength of the virtual forces.

The present work utilizes the method of continuously distributed dislocations to treat in closed form the screw dislocation pileup at a second phase of circular cross section and finite modulus.

This is the completely general case of the special cases depicted in Figure 1 and allows a simultaneous examination of size and rigidity effects. The size effect appears in variations of the parameter

$$\beta = \frac{L}{R} + 1, \quad (i)$$

and the rigidity effect appears in variations of the parameter

$$\kappa = \frac{G_2 - G_1}{G_2 + G_1}, \quad (ii)$$

where G_2 and G_1 are the shear moduli of the respective phases.

The method of continuously distributed dislocations provides a powerful analytical means of treating pileup problems in inhomogeneous media. Head and Louat⁽¹⁰⁾ have commented on the advantages of using the continuous distribution approach as compared to the discrete dislocation method used by Eshelby, Frank, and Nabarro.⁽¹⁾ The basic procedure used is the formulation of the pileup problem from the corresponding single dislocation solution, followed by the obtaining of the dislocation distribution function. Once the distribution function is known, the stress field is found by integrating the single dislocation stress field over the distribution of dislocations. It is interesting to note that the discrete⁽¹⁾ and the distributed⁽¹⁰⁾ solutions for the screw and edge pileups in a homogeneous medium yield almost identical results for the local stress field.

2. FORMULATION OF THE PROBLEM

Consider the infinite two-phase elastic medium depicted in Figure 2. Region 2 is a circular cylindrical inclusion of radius R and shear modulus G_2 which is imbedded in a matrix of shear modulus G_1 . The cylinder is infinitely long in the z -direction with the z -axis coinciding with the cylinder axis. Since we shall formulate a problem independent of z , we need only consider the x - y plane section in Figure 2. The elastic stress field of a single screw dislocation located at $(t,0)$ in the matrix is⁽⁶⁾:

$$\begin{aligned}
 \tau_{xz} &= -\frac{G_1 b}{2\pi} \left\{ \frac{y}{(x-t)^2 + y^2} + \kappa \left[\frac{y}{\left(x - \frac{R^2}{t}\right)^2 + y^2} - \frac{y}{x^2 + y^2} \right] \right\}, \\
 & \hspace{15em} (x^2 + y^2 > R^2); \\
 &= -\frac{G_1 b}{2\pi} (1+\kappa) \frac{y}{(x-t)^2 + y^2}, \\
 & \hspace{15em} (x^2 + y^2 < R^2); \\
 \\
 \tau_{yz} &= \frac{G_1 b}{2\pi} \left\{ \frac{x-t}{(x-t)^2 + y^2} + \kappa \left[\frac{x - \frac{R^2}{t}}{\left(x - \frac{R^2}{t}\right)^2 + y^2} - \frac{x}{x^2 + y^2} \right] \right\}, \\
 & \hspace{15em} (x^2 + y^2 > R^2); \\
 &= \frac{G_1 b}{2\pi} (1+\kappa) \frac{x-t}{(x-t)^2 + y^2}, \\
 & \hspace{15em} (x^2 + y^2 < R^2);
 \end{aligned} \tag{1}$$

where

$$\kappa = \frac{G_2 - G_1}{G_2 + G_1} \tag{2}$$

b is the dislocation Burgers' vector, which is parallel to the z -axis.

Perfect interface bonding has been assumed so that τ_{rz} and the

displacement field are continuous across the circle $x^2 + y^2 = R^2$. With these boundary conditions the stress field in the matrix is equivalent to the stress field in an infinite homogeneous medium of shear modulus G_1 containing the real dislocation at $(t, 0)$ and two virtual or image dislocations at $(R^2/t, 0)$ and the origin whose Burgers' vectors are κb and $-\kappa b$, respectively (Figure 2).

The problem of a linear array of length L containing N right-hand screw dislocations piled up against the inclusion under the application of an applied shear stress $\tau_{yz} = -\tau$ (Figure 3a) may be formulated as follows. For static equilibrium the force acting on any one dislocation in the pileup due to all the other pileup dislocations must balance the force due to the applied shear. This requires that

$$\frac{G_1 b}{2\pi} \left\{ \sum_{\substack{j=1 \\ j \neq i}}^N \frac{1}{x_i - x_j} + \kappa \sum_{j=1}^N \frac{1}{x_i - (R^2/x_j)} - \frac{\kappa N}{x_i} \right\} = \tau, \quad i = 1, 2, \dots, N. \quad (3)$$

Equation (3) represents N simultaneous equations to be solved for the x_i 's, the equilibrium positions of the pileup dislocations.

Equation (3) may be reinterpreted in terms of image dislocations as follows (Figure 3b). Considering an infinite homogeneous medium, the first sum on the left side of (3) represents the stress at x_i due to the other $N-1$ dislocations in the real pileup; the second sum, the stress at x_i due to a pileup of N image dislocations, each of strength κb , at positions $(R^2/x_j, 0)$ inside the circle $x^2 + y^2 = R^2$; the third term, the stress at x_i due to a giant image dislocation of Burgers' vector $-\kappa N b$ at the origin.

When N is large we may invoke the approximation of continuously distributed dislocations--i.e., replacing the discrete dislocations in the array by a continuous distribution of dislocations--and recast the equation of static equilibrium as a singular integral equation. Defining the dimensionless parameter $\lambda_i = x_i/R$ and using the distributed dislocation approximation, equation (3) becomes

$$\int_1^{\beta} \frac{f(\zeta) d\zeta}{\lambda - \zeta} + \kappa \int_1^{\beta} \frac{f(\zeta) d\zeta}{\lambda - \frac{1}{\zeta}} = \frac{\kappa N}{\lambda} + \frac{2\pi R\tau}{G_1 b}, \quad 1 < \lambda \leq \beta, \quad (4)$$

where

$$\beta = \frac{L}{R} + 1. \quad (5)$$

λ is a field point, ζ a source point anywhere in the distributed array, the first integral on the left is defined by its Cauchy principle value, and $f(\zeta)$ is the unknown dislocation distribution function.

3. SOLUTION OF THE INTEGRAL EQUATION

We shall consider the case of a pileup whose distribution function becomes infinite at the inclusion-pileup intersection. Hence, we seek a solution to (4) such that $f(\zeta)$ is unbounded (with a weak singularity) at $\zeta = 1$. At the trailing end of the pileup ($\zeta = \beta$) the distribution function must vanish. It will be shown that when $\kappa = -1$ (i.e., the case in which the second phase is a circular hole)

the distribution function will vanish at both ends of the array.

Discussion of this special case will be deferred until later.

Knowing the form of the distribution functions obtained in cases 3, 5, and 6 mentioned in the introduction, it is possible to guess the solution to equation (4). As a first trial let us guess a solution $f_0(\xi)$ of the form

$$f_0(\xi) = A\left(1 + \frac{1}{\xi^2}\right) \sinh \left\{ g \cosh^{-1} \left[\left(\frac{\beta-1}{\beta+1} \right) \left(\frac{\xi+1}{\xi-1} \right) \right] \right\} \\ + B\left(1 - \frac{1}{\xi^2}\right) \sinh \left\{ w \cosh^{-1} \left[\left(\frac{\beta-1}{\beta+1} \right) \left(\frac{\xi+1}{\xi-1} \right) \right] \right\}. \quad (6)$$

This particular form is chosen for the following reason. The distribution functions found by Chou,⁽⁵⁾ Barnett and Tetelman,⁽⁸⁾ and Barnett⁽⁹⁾ were of the form

$$f(\xi) = a_0 \cosh^{-1} \left(\frac{L}{\xi} \right) \quad (\text{Chou: } \kappa = 1, \beta = 1) \quad (7a)$$

$$f(\xi) = b_0 \sinh \left\{ g_0 \cosh^{-1} \left(\frac{L}{\xi} \right) \right\} \quad (\text{Barnett: } \beta = 1, -1 < \kappa \leq 1) \quad (7b)$$

$$f(\xi) = c_0 \left(1 + \frac{1}{\xi^2} \right) \cosh^{-1} \left[\left(\frac{\beta-1}{\beta+1} \right) \left(\frac{\xi+1}{\xi-1} \right) \right] \\ + d_0 \left(1 - \frac{1}{\xi^2} \right) \sinh \left\{ \cosh^{-1} \left[\left(\frac{\beta-1}{\beta+1} \right) \left(\frac{\xi+1}{\xi-1} \right) \right] \right\} \quad (7c)$$

(Barnett & Tetelman: $\kappa = 1, 1 \leq \beta < \infty$).

Thus, the forms of equations (7a) and (7b) lead one to generate the trial function of equation (6) from equation (7c). The constants A, B, g, and w in (6) are as yet undetermined.

Making the substitution $u = \cosh^{-1} \left[\left(\frac{\beta-1}{\beta+1} \right) \left(\frac{\zeta+1}{\zeta-1} \right) \right]$,

$$\begin{aligned}
 & \left\{ \int_1^\beta \frac{f_0(\zeta) d\zeta}{\lambda - \zeta} \right. \\
 & \left. \int_1^\beta \frac{f_0(\zeta) d\zeta}{\lambda - \frac{1}{\zeta}} \right\} \\
 &= 2A \frac{\beta+1}{\beta-1} \int_{-\infty}^{\infty} \left[\frac{\sinh gu \sinh u du}{\left[\frac{\beta+1}{\beta-1} \cosh u \pm 1 \right]} \left[1 + \frac{2}{\left[\frac{\beta+1}{\beta-1} \right]^2 \cosh^2 u - 1} \right] \right. \\
 & \quad \left. \times \frac{1}{\frac{\beta+1}{\beta-1} (\lambda-1) \cosh u \mp (1+\lambda)} \right] \\
 & + 4B \left(\frac{\beta+1}{\beta-1} \right)^2 \int_{-\infty}^{\infty} \left[\frac{\sinh wu \sinh u \cosh u du}{\left[\frac{\beta+1}{\beta-1} \cosh u \pm 1 \right]^2 \left[\frac{\beta+1}{\beta-1} \cosh u \mp 1 \right]} \right. \\
 & \quad \left. \times \frac{1}{\frac{\beta+1}{\beta-1} (\lambda-1) \cosh u \mp (1+\lambda)} \right] \tag{8} \\
 &= \left\{ \int_{-\infty}^{\infty} I_1(u, \lambda) du \right. \\
 & \left. \int_{-\infty}^{\infty} I_2(u, \lambda) du \right\} .
 \end{aligned}$$

Considering

$$\oint_C I_1(u, \lambda) du , \tag{9}$$

where C is the indented rectangle in the complex $u = v + i\Omega$ plane (Figure 4), letting $v_0 \rightarrow \infty$, $\epsilon \rightarrow 0$, and applying the Cauchy residue theorem, one finds that if we let (see Appendix)

$$\left. \begin{aligned}
 g &= \frac{2}{\pi} \sin^{-1} \sqrt{\frac{1-\kappa}{2}} \\
 w &= \frac{2}{\pi} \sin^{-1} \sqrt{\frac{1+\kappa}{2}} = 1 - g \\
 \gamma_0 &= \cos^{-1} \frac{\beta-1}{\beta+1}, \quad 0 \leq \gamma_0 \leq \frac{\pi}{2} \\
 A &= \frac{2R\tau}{G_1 b} \frac{\sin w(\pi - \gamma_0)}{\sqrt{1-\kappa^2} \sin \gamma_0} \\
 B &= \frac{2R\tau}{G_1 b} \frac{\sin g(\pi - \gamma_0)}{\sqrt{1-\kappa^2} \sin \gamma_0}
 \end{aligned} \right\} \quad (10)$$

then $f_0(\zeta)$ satisfies the integral equation

$$\int_1^\beta \frac{f_0(\zeta) d\zeta}{\lambda - \zeta} + \kappa \int_1^\beta \frac{f_0(\zeta) d\zeta}{\lambda - \frac{1}{\zeta}} = \frac{\kappa N_0}{\lambda} + \frac{2\pi R\tau}{G_1 b} - \frac{\alpha_0}{\lambda}, \quad (11)$$

where

$$N_0 = \int_1^\beta f_0(\zeta) d\zeta, \quad (12)$$

$$\alpha_0 = \kappa N_0 - \frac{2\pi}{\sin \gamma_0} \frac{\beta-1}{\beta+1} \{g A \cos g(\pi - \gamma_0) - wB \cos w(\pi - \gamma_0)\}$$

If α_0 were identically zero, then $f_0(\zeta)$ would be a solution to equation (4). This is not the case, so we must find a distribution function $f_1(\zeta)$ satisfying

$$\int_1^\beta \frac{f_1(\zeta) d\zeta}{\lambda - \zeta} + \kappa \int_1^\beta \frac{f_1(\zeta) d\zeta}{\lambda - \frac{1}{\zeta}} = \frac{\kappa N_1}{\lambda} + \frac{\alpha_0}{\lambda}, \quad (13)$$

where

$$N_1 = \int_1^\beta f_1(\zeta) d\zeta.$$

Then $f_0(\zeta) + f_1(\zeta)$ will be the required solution to equation (4).

A suitable guess for $f_1(\zeta)$ is

$$f_1(\zeta) = \frac{C}{\zeta} \sinh \left\{ g \cosh^{-1} \left[\left(\frac{\beta-1}{\beta+1} \right) \left(\frac{\zeta+1}{\zeta-1} \right) \right] \right\}. \quad (14)$$

Again making the substitution $u = \cosh^{-1} \left[\left(\frac{\beta-1}{\beta+1} \right) \left(\frac{\zeta+1}{\zeta-1} \right) \right]$ and using the technique illustrated in equations (8) and (9), $f_1(\zeta)$ is a solution to (13) if

$$C = - \frac{2}{\sin \gamma_0} \frac{\cos \gamma_0}{\cos g\gamma_0} \{ gA \sin g\gamma_0 - wB \sin w\gamma_0 \}. \quad (15)$$

Thus, in dimensionless form, the exact distribution function is

$$\begin{aligned}
f(\zeta) &= \frac{2R\tau}{G_1 b} \frac{1}{\sqrt{1-\kappa^2}} \frac{1}{\sin \gamma_0} \\
&\times \left\{ \left(1 + \frac{1}{\zeta^2}\right) \sin w(\pi - \gamma_0) \sinh g\eta_0 \right. \\
&\quad + \left(1 - \frac{1}{\zeta^2}\right) \sin g(\pi - \gamma_0) \sinh w\eta_0 \\
&\quad - \frac{2}{\sin \gamma_0} \frac{\cos \gamma_0}{\cos g\gamma_0} \left[g\sqrt{1-\kappa^2} \sin \gamma_0 - \sin g(\pi-\gamma_0) \sin w\gamma_0 \right] \\
&\quad \left. \times \frac{1}{\zeta} \sinh g\eta_0 \right\}, \tag{16}
\end{aligned}$$

where

$$\begin{aligned}
\eta_0 &= \cosh^{-1} \left[\left(\frac{\beta-1}{\beta+1}\right) \left(\frac{\zeta+1}{\zeta-1}\right) \right] \\
0 \leq \gamma_0 &= \cos^{-1} \frac{\beta-1}{\beta+1} \leq \frac{\pi}{2} \tag{17} \\
g &= \frac{2}{\pi} \sin^{-1} \sqrt{\frac{1-\kappa}{2}} = 1 - w.
\end{aligned}$$

The number of dislocations in the pileup is then given as

$$N = \frac{\pi\tau L}{G_1 b} \frac{1}{\sqrt{1-\kappa^2}} \frac{\beta+1}{\beta} \frac{1}{\cos g\gamma_0} \left[g \sin w(\pi-\gamma_0) + w \sin g(\pi-\gamma_0) \cos \gamma_0 \right] \tag{18}$$

The limiting cases $\kappa \rightarrow 1, 0$ and $\beta \rightarrow 1, \infty$ check all previous solutions. (5,8,9,10) One should note that the true distribution function in dimensional form is

$$f(\zeta)_{\text{true}} = \frac{1}{R} f(\zeta). \tag{19}$$

Figures 5, 6, and 7 show the true distribution function plotted as a function of $\xi_0 = \rho_0/L$ (for fixed κ and variable β , and vice-versa), where ρ_0 is the distance from the leading edge of the pileup to any point in the array. The relation between ξ and ξ_0 is

$$\xi = 1 + (\beta-1) \xi_0 \quad (0 \leq \xi_0 \leq 1) \quad (20)$$

Figure 8 is a three-dimensional view of the surface $\tau L/G_1 bN$ as a function of inclusion size (β) and rigidity (κ). $1/N$ has been plotted rather than N for two reasons:

- (1) Previous treatments^(5,9) have elected to plot $1/N$ versus κ (for $\beta = 1$) because of the very linear relation obtained when $0 \leq \kappa \leq 1$.
- (2) When $\kappa < 0$ and $\kappa \rightarrow -1$, N becomes large. By plotting $1/N$, the entire rigidity range $-1 < \kappa \leq 1$ may be depicted more easily.

As particle size decreases (i.e., as β becomes large), the $\tau L/G_1 bN$ surface approaches the plane $\tau L/G_1 bN = 1/\pi$, independent of the value of κ . Figures 9 and 10 represent sections through the surface at constant β and at constant κ .

4. THE PILEUP STRESS FIELD

The stress field of the piled up array is found by integrating the stress field of a single dislocation (equation (1)) over the distribution, i.e.,

$$\tau_{ij}(x,y) = \int_R^{L+R} \tau_{ij}(x,y,\zeta) f(\zeta) d\zeta \quad (21)$$

The integrals are somewhat involved, but they may be evaluated by an integration in the complex plane.^(8,9) Expressions for special cases of the stress field are presented below:

(a) The shear stress τ_{rz} along the inclusion interface:

$$\begin{aligned} \tau_{rz} = & - \frac{\tau}{\sin \gamma_0} \sqrt{\frac{2}{1-\kappa}} \\ & \times \left\{ \sin w(\pi-\gamma_0) [(\sinh gv_0) \cos \theta + \sin g(\frac{\pi}{2} - \gamma_0) \sin \theta] \right. \\ & + \sin g(\pi-\gamma_0) \sin \theta [\cosh wv_0 - \cos w(\frac{\pi}{2} - \gamma_0)] \\ & - \frac{\cos \gamma_0}{\sin \gamma_0 \cos g\gamma_0} \left[g\sqrt{1-\kappa^2} \sin \gamma_0 - \sin g(\pi-\gamma_0) \sin w\gamma_0 \right] \\ & \left. \times \sinh gv_0 \right\} , \quad (20) \end{aligned}$$

where

$$v_0 = \sinh^{-1} \left\{ \left(\frac{\beta-1}{\beta+1} \right) \cot \frac{\theta}{2} \right\} , \quad (21)$$

and θ is the polar angle measured from the center of the inclusion (Figure 3a).

(b) The shear stress τ_{yz} on the slip plane $y = 0$ inside the inclusion:

When $\frac{1}{\beta} \leq \lambda = \frac{x}{R} \leq 1$,

$$\begin{aligned} \tau_{yz} = & \frac{\tau}{(1-\kappa) \sin \gamma_0} \\ & \times \left\{ \left(1 + \frac{\kappa}{\lambda^2}\right) \sin \gamma_0 \right. \\ & + \frac{2 \cos \gamma_0}{\lambda \cos g\gamma_0 \sin \gamma_0} \left[g \sqrt{1-\kappa^2} \sin \gamma_0 - \sin g(\pi-\gamma_0) \sin w\gamma_0 \right] \\ & \times \cosh g\eta_1 \\ & - \left[\sin w(\pi-\gamma_0) \left(1 + \frac{1}{\lambda^2}\right) \cosh g\eta_1 \right. \\ & \left. \left. + \sin g(\pi-\gamma_0) \left(1 - \frac{1}{\lambda^2}\right) \cosh w\eta_1 \right] \right\} \quad (22) \end{aligned}$$

where

$$\eta_1 = \cosh^{-1} \left\{ \left(\frac{\beta-1}{\beta+1}\right) \left(\frac{\lambda+1}{1-\lambda}\right) \right\}. \quad (23)$$

For $-1 \leq \lambda = \frac{x}{R} \leq \frac{1}{\beta}$, the same equation is valid with $\cosh g\eta_1$ and $\cosh w\eta_1$ replaced by $\cos g\eta_2$ and $\cos w\eta_2$, respectively, where

$$0 \leq \eta_2 = \cos^{-1} \left\{ \left(\frac{\beta-1}{\beta+1}\right) \left(\frac{\lambda+1}{1-\lambda}\right) \right\} \leq \frac{\pi}{2}. \quad (24)$$

Figure 11 shows a three dimensional view of this stress near the pileup tip as a function of $\rho/L = (1-\lambda)/(\beta-1)$ (see Figure 3a)

and inclusion size β . Each of the three stress surfaces shown corresponds to a different value of inclusion rigidity (κ). Figure 12 shows a section taken through Figure 11 at constant β .

(c) The shear stress τ_{yz} on the slip plane $y = 0$ outside the inclusion ($\lambda = \frac{x}{R} \leq -1$):

$$\begin{aligned} \tau_{yz} = & \frac{\tau}{\sqrt{1-\kappa^2} \sin \gamma_0} \\ & \times \left\{ \sqrt{1-\kappa^2} \sin \gamma_0 \right. \\ & + \frac{2}{\lambda} \frac{\cos \gamma_0}{\cos g\gamma_0 \sin \gamma_0} \left[g\sqrt{1-\kappa^2} \sin \gamma_0 - \sin g(\pi-\gamma_0) \sin w\gamma_0 \right] \\ & \times \sin g\sigma_0 \\ & - \left[\left(1 + \frac{1}{\lambda^2}\right) \sin w(\pi-\gamma_0) \sin g\sigma_0 \right. \\ & \left. \left. + \left(1 - \frac{1}{\lambda^2}\right) \sin g(\pi-\gamma_0) \sin w\sigma_0 \right] \right\}, \end{aligned} \quad (25)$$

where

$$0 \leq \sigma_0 = \cos^{-1} \left\{ \left(\frac{\beta-1}{\beta+1} \right) \left(\frac{|\lambda|-1}{|\lambda|+1} \right) \right\} \leq \frac{\pi}{2}. \quad (26)$$

5. DISCUSSION

One readily notes that the expressions for the special stresses given in equations (20), (22), and (26) are extremely cumbersome, and it is useful to have approximate expressions for the stress field in the second phase close to the pileup tip ($L/\rho \gg 1$). For $\kappa \neq \pm 1$ these local stresses are found to be:

$$\left. \begin{aligned} \frac{\tau_{XZ}}{\tau} &\sim A(\kappa, \beta) \left\{ \frac{4}{\beta+1} \frac{L}{\rho} \right\}^{\beta} \frac{\beta+1}{2\sqrt{\beta}} \sin g\phi \\ \frac{\tau_{YZ}}{\tau} &\sim -A(\kappa, \beta) \left\{ \frac{4}{\beta+1} \frac{L}{\rho} \right\}^{\beta} \frac{\beta+1}{2\sqrt{\beta}} \cos g\phi \end{aligned} \right\} \quad (27)$$

where

$$A(\kappa, \beta) = \frac{\sin w(\pi - \gamma_0) \sin w\gamma_0 + w\sqrt{1-\kappa^2} \cos \gamma_0 \sin \gamma_0}{(1-\kappa) \sin \gamma_0 \cos g\gamma_0} \quad (28)$$

ϕ is the polar angle in the second phase relative to the pileup tip, and ρ is the associated radius vector (Figure 3a). As $\kappa \rightarrow 1$, the stresses near the pileup tip diverge logarithmically. (5,8,9)

Now let us examine equation (27) for cases in which the particle diameter $2R$ is much greater and much less than the slip line length L . Since

$$\frac{4}{\beta+1} \frac{L}{\rho} = \frac{4R}{L+2R} \cdot \frac{L}{\rho}, \quad (29)$$

$$\frac{4}{\beta+1} \frac{L}{\rho} \approx \frac{2L}{\rho} \quad \text{when} \quad \frac{L}{R} \ll 2 \quad (30)$$

and

$$\frac{4}{\beta+1} \frac{L}{\rho} \approx \frac{4R}{\rho} \quad \text{when} \quad \frac{L}{R} \gg 2 .$$

Hence, when $L/\rho \gg 1$ and $\kappa \neq \pm 1$

$$\left. \begin{aligned} \frac{\tau_{xz}}{\tau} &\sim A(\kappa, \beta) \left(\frac{2L}{\rho}\right)^g \sin g\phi \\ \frac{\tau_{yz}}{\tau} &\sim -A(\kappa, \beta) \left(\frac{2L}{\rho}\right)^g \cos g\phi \end{aligned} \right\} \frac{L}{R} \ll 2 \quad (31)$$

or

$$\left. \begin{aligned} \frac{\tau_{xz}}{\tau} &\sim A(\kappa, \beta) \sqrt{\frac{L}{4R}} \left\{\frac{4R}{\rho}\right\}^g \sin g\phi = A(\kappa, \beta) \sqrt{\frac{L}{\rho}} \left\{\frac{4R}{\rho}\right\}^{g-1/2} \sin g\phi \\ \frac{\tau_{yz}}{\tau} &\sim -A(\kappa, \beta) \sqrt{\frac{L}{4R}} \left\{\frac{4R}{\rho}\right\}^g \cos g\phi = -A(\kappa, \beta) \sqrt{\frac{L}{\rho}} \left\{\frac{4R}{\rho}\right\}^{g-1/2} \cos g\phi \end{aligned} \right\} \frac{L}{R} \gg 2 \quad (32)$$

where

$$0 < g = \frac{2}{\pi} \sin^{-1} \sqrt{\frac{1-\kappa}{2}} < 1 . \quad (33)$$

One notes that

- (a) The exponent g is independent of particle size and depends only upon the ratio G_2/G_1 .
- (b) In the case of particles which are large relative to the slip line length, particle size affects stresses only through the constant $A(\kappa, \beta)$. The relevant term in the expression for local stress intensification is $(2L/\rho)^g$, and this is the

same term which would appear if the second phase were semi-infinite. This is physically reasonable since when $L/R \ll 2$, the second phase is extremely planar near the pileup tip and the leading dislocations in the pileup do not sense the finite size of the inclusion.

- (c) In the case of particles which are small relative to the slip line length, the relevant term in the expression for the local stresses is $\sqrt{\frac{L}{\rho}} \left(\frac{4R}{\rho}\right)^{g-1/2}$. The factor $\sqrt{\frac{L}{\rho}}$ is the same term which appears in the calculations based upon a homogeneous medium (no particle present), so that the term $\left(\frac{4R}{\rho}\right)^{g-1/2}$ may be viewed as a correction term introduced by the finite size and rigidity of the second phase.

We can use equations (31) and (32) to illustrate size and rigidity effects upon the local stresses by two sample calculations which will be compared with similar calculations assuming the absence of the inclusion. Since the maximum shear stress acting along any plane occurs upon the slip plane $y = 0$, we shall concern ourselves with the stress $\tau_{yz}|_{y=0}$ near the pileup tip inside the second phase.

Case 1: $L \simeq 10^{-4}$ cm, $R \simeq 2 \times 10^{-4}$ cm (a typical cermet)

$$(i) \quad \frac{G_2}{G_1} = 5, \quad \kappa = \frac{2}{3}$$

$$\frac{\tau_{yz}}{\tau} \simeq - \left\{ \begin{array}{c} 17.5 \\ 7.2 \\ 4.5 \end{array} \right\} \quad \text{for} \quad \rho = \left\{ \begin{array}{c} 10^{-7} \\ 10^{-6} \\ 10^{-5} \end{array} \right\} \text{ cm} .$$

$$(ii) \quad \kappa = 0 \quad (\text{no inclusion})$$

$$\frac{\tau_{yz}}{\tau} \approx - \left\{ \begin{array}{c} 45 \\ 14 \\ 4.5 \end{array} \right\} \quad \text{for} \quad \rho = \left\{ \begin{array}{c} 10^{-7} \\ 10^{-6} \\ 10^{-5} \end{array} \right\} \text{ cm} .$$

Thus, when $\kappa > 0$, the local stresses in large particles may be lower than those predicted by homogeneous elasticity by a factor of 2 or 3 when $\rho \geq 10\overset{\circ}{\text{A}}$. This is essentially a rigidity effect, since R , the particle size, has little effect upon the local stresses when $L/R \ll 2$. We shall not consider $\kappa < 0$ in this calculation, because if $G_2 < G_1$, slip should occur inside the particle before the matrix yields.

Case 2: $L \geq \approx 10^{-5}$ cm, $R \leq 5 \times 10^{-6}$ cm.

The essential difference between the local stress field in the particle and that in a homogeneous medium is given by the correction factor $(4R/\rho)^{g-1/2}$ in equation (32). This correction factor is plotted in Figure 13 for two different size particles and two different relative rigidities. The correction factor becomes appreciable at distances ρ from the pileup tip which are less than $10\overset{\circ}{\text{A}}$. However, it is doubtful that much physical significance can be attached to this range of ρ values. At distances from the pileup tip which are physically significant ($\rho \geq 25\overset{\circ}{\text{A}}$), when $\kappa > 0$, the correction factor may vary from about 1/2 to 1/3, so that the local stresses in the particle are about 2 or 3 times lower than those predicted by homogeneous elasticity theory. This may prove significant when one begins to examine relaxation of the high local stresses by either particle or particle interface fracture, cross slip of the blocked dislocations around the particle, or induced slip in the matrix.

These effects upon the local stresses near the pileup tip may be easily understood by using the concept of image dislocation forces. When $\kappa > 0$, decreasing the particle size effectively decreases the repulsive image forces near the pileup tip by allowing the giant image dislocation at the origin (Figure 3b) to partially cancel out the effect of the image pileup. Thus, the distribution of dislocations near the pileup tip is increased, and local stresses in the second phase are increased as particle size decreases. When $\kappa < 0$, decreasing the particle size decreases the attractive image forces near the pileup tip, and the same reasoning allows us to conclude that local stresses in the second phase should decrease with decreasing particle size. These conclusions are borne out in Figure 11. The effect of rigidity (κ) is explained in the same fashion. Local stresses in the second phase always decrease as the second phase rigidity increases. An increase in κ

- (1) increases the repulsive image forces nearest the pileup tip when $\kappa > 0$
- (2) decreases the attractive image forces nearest the pileup tip when $\kappa < 0$.

In both cases the net effect of an increase in rigidity is to decrease the distribution of pileup dislocations near the second phase and hence lower the local stress field in the inclusion.

Figures 8, 9, and 10 indicate that the effect of particle size upon N , the number of dislocations in the pileup, is small, at least when $\kappa > 0$. Neither changes in β nor κ can change N by more than 50% when $\kappa > 0$.

When $\kappa = -1$ the second phase becomes a circular hole. Using L'Hospital's rule in equation (16), the true distribution function for the hole becomes

$$f(\zeta) = \frac{2\tau}{\pi G_1 b} \frac{\zeta-1}{\zeta^2} \left\{ \left[\frac{\pi}{2} + \sin^{-1} \frac{\beta-1}{\beta+1} \right] \sqrt{(\beta-\zeta)\left(\zeta - \frac{1}{\beta}\right)} + (\zeta+1) \cosh^{-1} \left[\left(\frac{\beta-1}{\beta+1} \right) \left(\frac{\zeta+1}{\zeta-1} \right) \right] \right\}. \quad (34)$$

This distribution is depicted in Figure 14 for different L/R ratios, and one notes that for the hole the distribution function is bounded at both ends of the array. As $\beta \rightarrow 1$ (i.e., $R \rightarrow \infty$ and the interface becomes a free planar surface) the distribution function becomes zero. In reality the integral equation (4) does not have an admissible solution in this case.⁽⁹⁾

The shear stress on the slip plane $y = 0$ outside the hole ($\lambda = x/R \leq -1$) is

$$\tau_{yz} = \tau \left\{ 1 + \frac{\lambda-1}{\lambda^2} \frac{\pi-\gamma_0}{\pi} \sqrt{(\beta-\lambda)\left(\frac{1}{\beta} - \lambda\right)} - \left(1 - \frac{1}{\lambda^2}\right) \frac{\sigma_0}{\pi} \right\}, \quad (35)$$

where σ_0 is as defined in equation (27). This stress is depicted in Figure 15.

The inability to obtain a solution to equation (4) (for $\kappa = -1$) which is unbounded at $\zeta = 1$ with a weak singularity is presently unexplained. Perhaps this is due to the fact that the

condition for pileup formation is that the leading dislocation be locked in position by a force strong enough to keep it from penetrating the second phase. The present and previous treatments have been able to neglect this force in the integral equation of static equilibrium--i.e., the locked dislocation was "smeared out" along with the trailing dislocations in the array--and still obtain a solution. However, in the case of a hole, the attractive image forces exerted by the free surface are at their strongest (as compared to $\kappa \neq -1$), and it is possible that one must include the locking force on the leading dislocation in equation (4) in order to obtain a solution.

The problem which has been treated in the present paper illustrates the difficulty involved in treating stress concentrations in inhomogeneous media, even for rather simple second phase geometries. The only alternative treatments available at present seem to be

- (1) The conformal mapping technique of Webster and Johnson⁽¹¹⁾ and Johnson.⁽¹²⁾
- (2) The standard boundary value problem approach of elasticity--i.e., the partial differential equation approach.

Unfortunately, both alternatives must consider the boundary conditions at the second phase interface which will usually be of the "dielectric" variety--i.e., continuity of the displacement field and combinations of its derivatives across the boundary. Problems of this type do not lend themselves easily to solution by conformal mapping, and it is possible that either alternative approach will require solution of an integral equation or possibly dual integral equations.

The beauty of the continuously distributed approach is that the boundary conditions for the distributed array will be satisfied automatically provided the solution for a single dislocation satisfying boundary conditions is known. In the case of screw dislocations in inhomogeneous media the close analogy with two-dimensional electrostatic charges in media of differing dielectric constants may often allow the single dislocation solution to be found rather easily.

Three limitations of the approach are:

- (1) Plastic relaxation by slip in the matrix or in the second phase has not been allowed during pileup formation. Stress relaxation can, however, be considered once the pileup has formed and the local stresses are known.
- (2) The case of a broadened slip band containing more than one linear array cannot be treated exactly, except for the case of an infinite sequence of screw arrays stacked on parallel slip planes and piled up against a semi-infinite second phase of finite rigidity.⁽¹³⁾
- (3) At present problems involving edge dislocation pileups cannot be treated because the single edge solutions,^(4,7) even for simple second phase geometries, are too complex in the elastic constants. Because the strain field of the edge has an associated dilatation, Poisson's ratio effects are encountered, and image edge dipoles and quadrupoles are needed to satisfy boundary conditions. The pileup equilibrium condition in this case becomes a singular integro-differential equation

which has not been solved. A preliminary investigation⁽¹³⁾ indicates that the distribution function obtained for the screw pileup at a semi-infinite second phase⁽⁹⁾ may suffice for the corresponding edge array problem for certain values of the respective elastic constants of the two phases.

It is also worth noting that although the present work and the previously mentioned treatments have examined pileups blocked at the inclusion, the same techniques should prove successful in treating the case in which a linear dislocation array approaches a second phase but is separated from the inhomogeneity by a finite distance.

ACKNOWLEDGMENTS

The authors wish to thank Miss Vaiva Pukite for performing the necessary computations on the Burroughs B5500 computer at the Stanford Computation Center. This research was supported by NASA grant NSG-622.

REFERENCES

1. Eshelby, J. D., Frank, F.C., and Nabarro, F.R.N., Phil. Mag., 42, 351 (1951).
2. Stroh, A.N., Proc. Roy. Soc., A 223, 404 (1954).
3. Bilby, B.A., Bullough, R., and Smith, E., Proc. Roy. Soc., A 231, 263 (1965).
4. Head, A.K., Proc. Phys. Soc. London, 66B, 793 (1953), and Phil. Mag., 44, 92 (1953).
5. Chou, Y.T., Acta Met., 13, 779 (1965).
6. Dundurs, J., private communication (1965).
7. Dundurs, J. and Mura, T., J. Mech. Phys. Solids, 12, 177, 1964.
8. Barnett, D.M. and Tetelman, A.S., to be published in J. Mech. Phys. Solids.
9. Barnett, D.M., to be published in Acta Met.
10. Head, A.K. and Louat, N., Aust. J. Phys., 8, 1 (1955).
11. Webster, L.D. and Johnson, H.H., J. App. Phys., 36, #6, 1927 (1965).
12. Johnson, H.H., J. App. Phys., 37, #4, 1763 (1966).
13. Barnett, D.M. and Tetelman, A.S., to be published.

$$\beta = \frac{L}{R} + 1 ; K = \frac{G_2 - G_1}{G_2 + G_1}$$

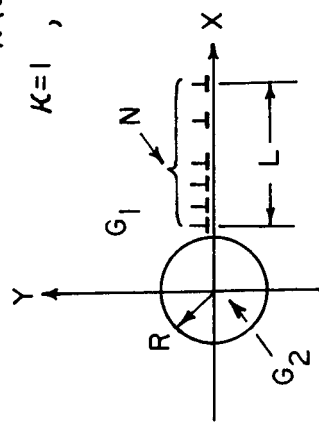
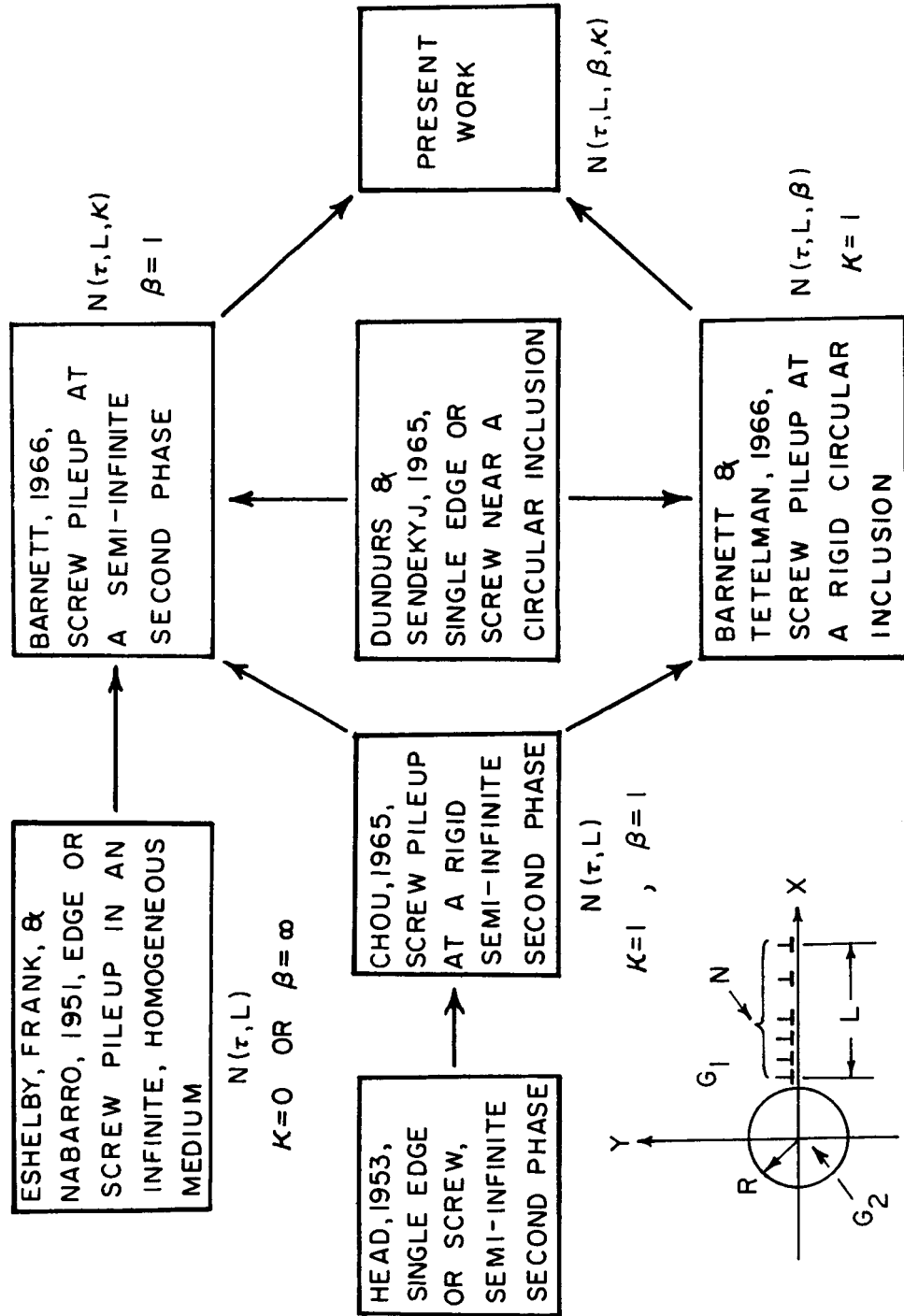


FIGURE 1: Flow Diagram Indicating Previous Analytical Treatments of Single Dislocations and Dislocation Pileups in Inhomogeneous Elastic Media.

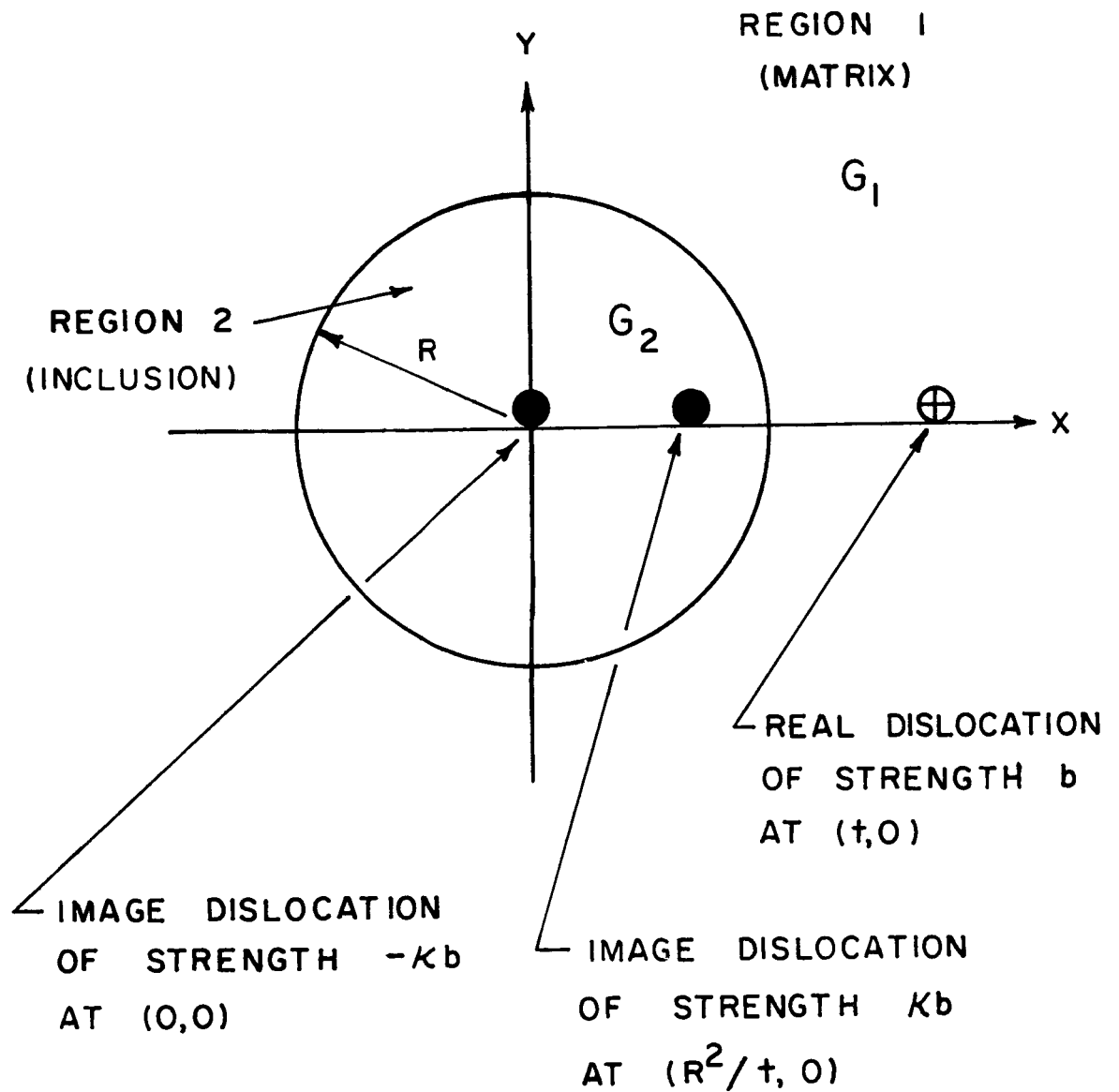


FIGURE 2: Schematic Illustration of Co-Ordinate System and the Equivalent Image Dislocation Arrangement Used to Describe the Stress Field of a Screw Dislocation Near a Circular Inclusion.

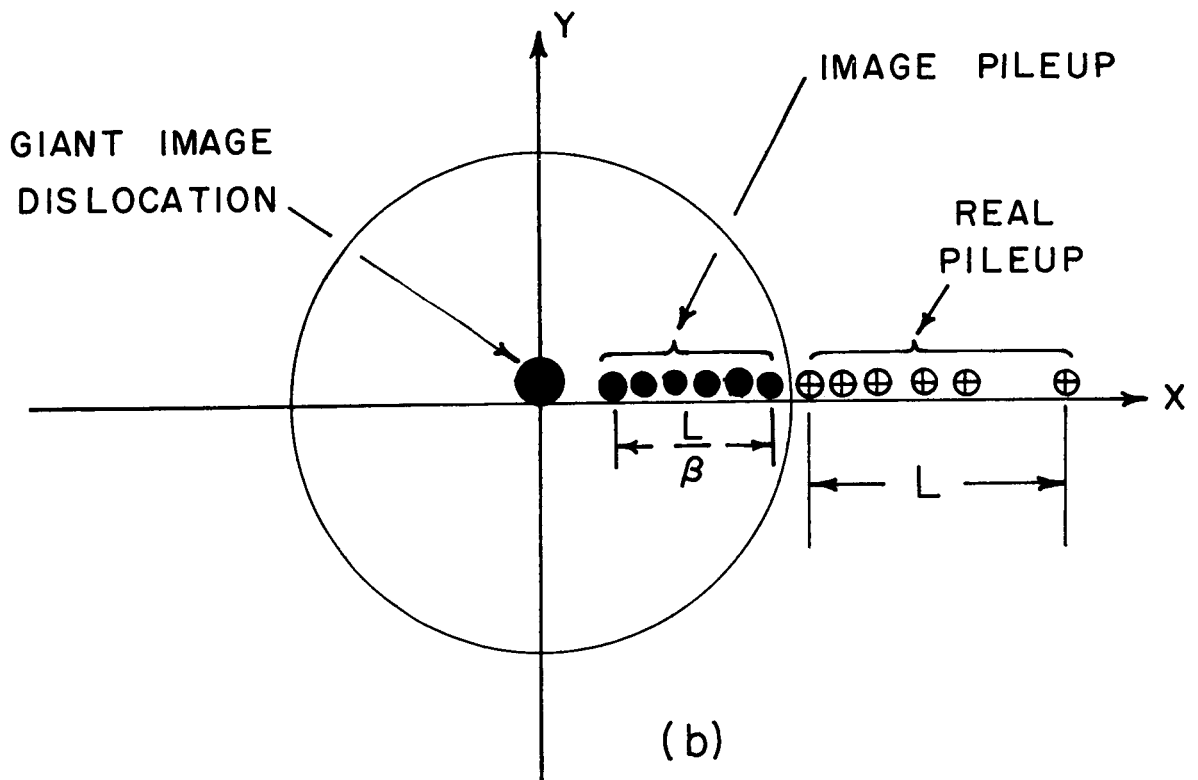
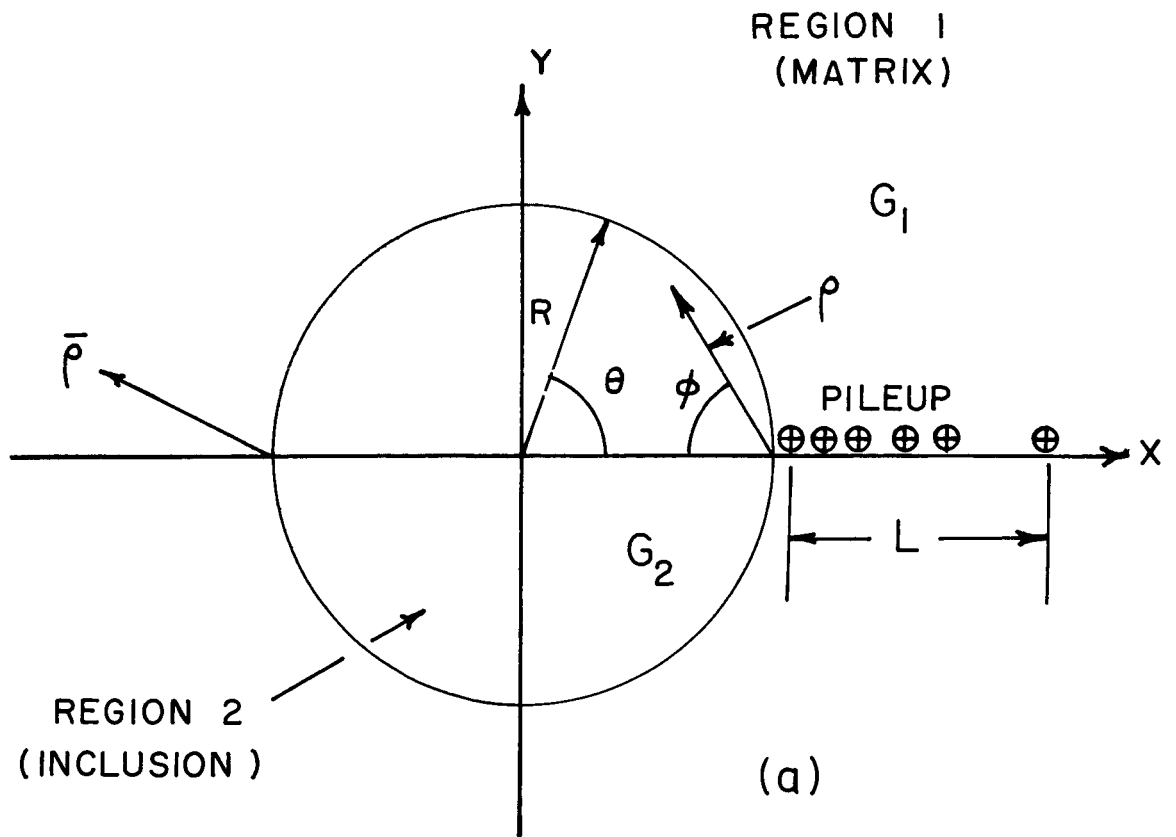


FIGURE 3: (a) Schematic Illustration of a Screw Dislocation Pileup Against a Circular Inclusion. (b) Schematic Illustration Showing Equivalent Image Dislocation System Used to Describe the Stress Field of the Pileup.

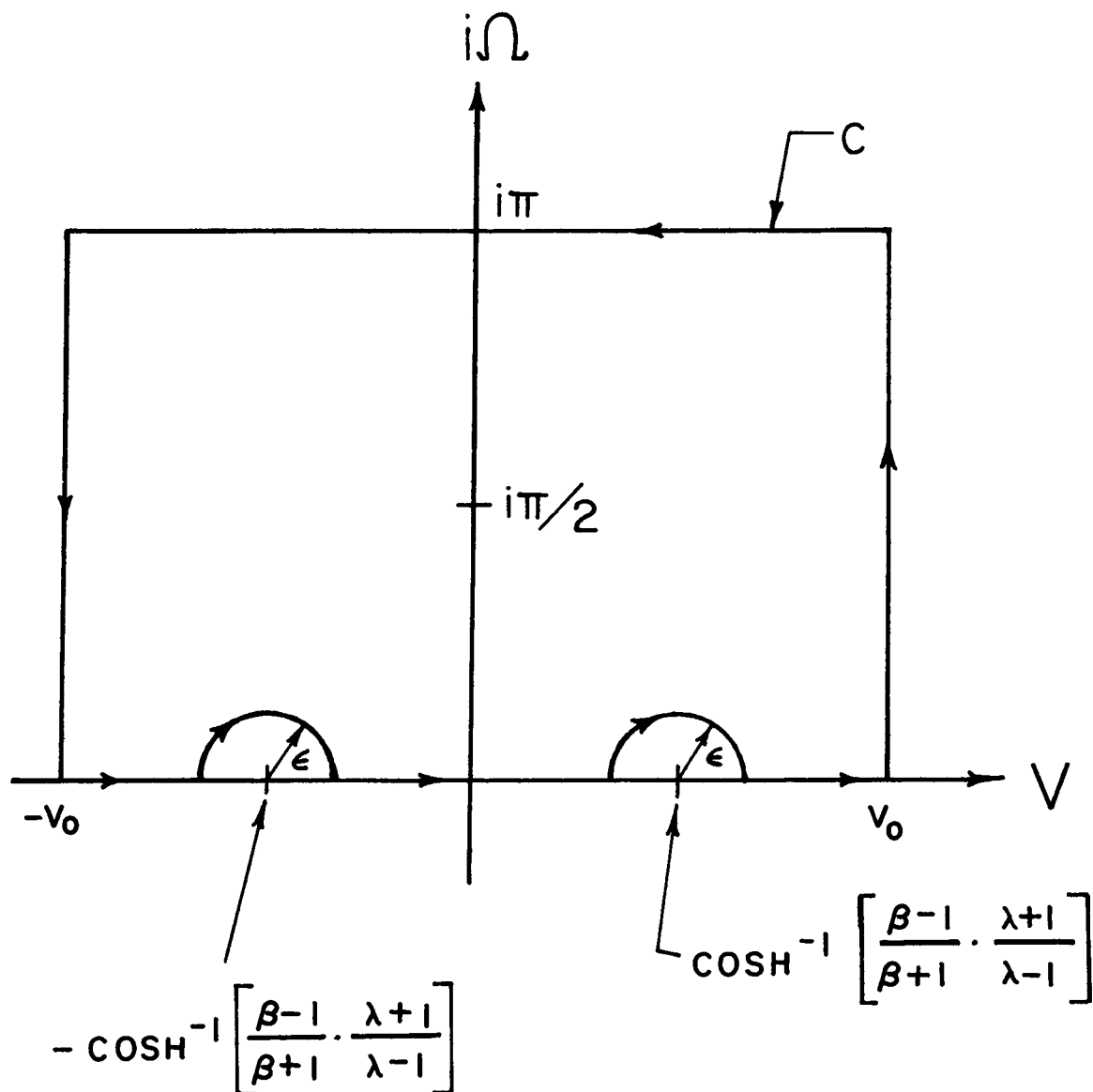


FIGURE 4: The Contour C in the complex $u = v + i\Omega$ Plane Used to Solve the Integral Equation for the Dislocation Distribution Function.

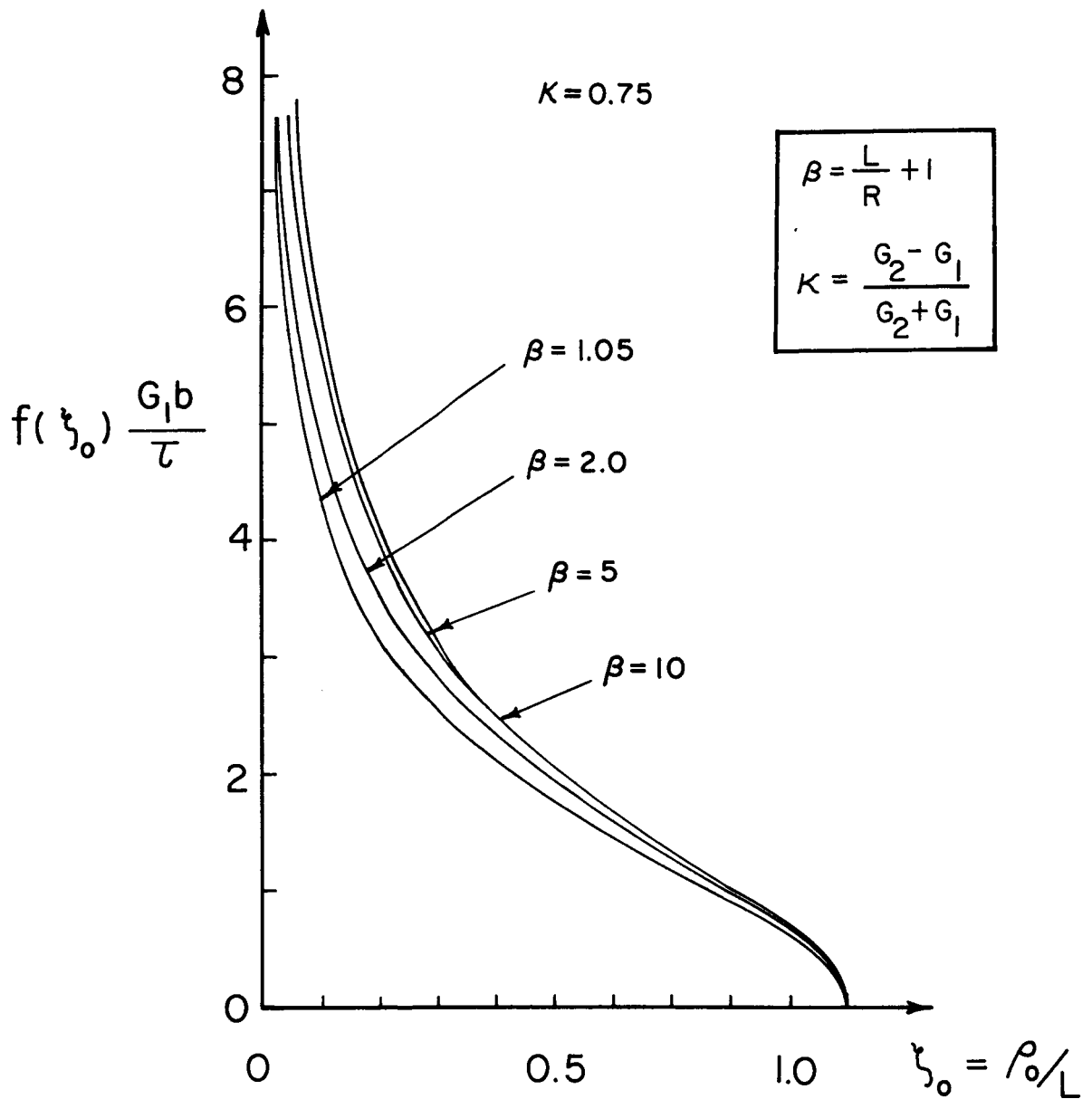


FIGURE 5: $f(\xi_0)$, The Dislocation Distribution Function, vs. $\xi_0 = \rho_0/L$ for a Fixed Relative Rigidity (κ) and Various L/R Ratios. The Pileup is in the Softer Phase ($G_2 > G_1$). ρ_0 is the Distance from the Leading Edge to the Pileup to any Point in the Array.

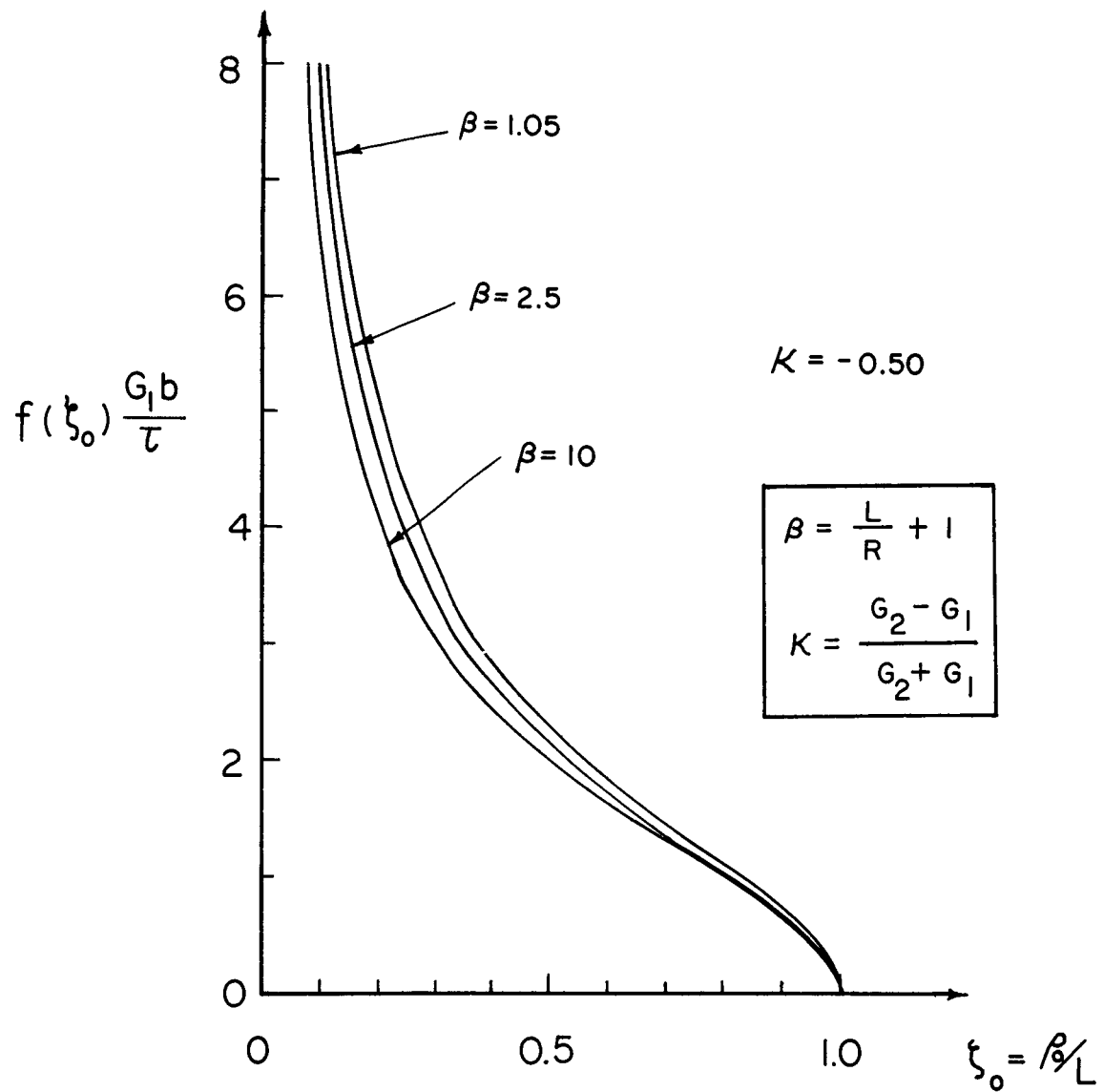


FIGURE 6: $f(\xi_0)$, The Dislocation Distribution Function, vs. $\xi_0 = \rho_0/L$ for a Fixed Relative Rigidity (κ) and Various L/R Ratios. The Pileup is in the Harder Phase ($G_2 < G_1$).

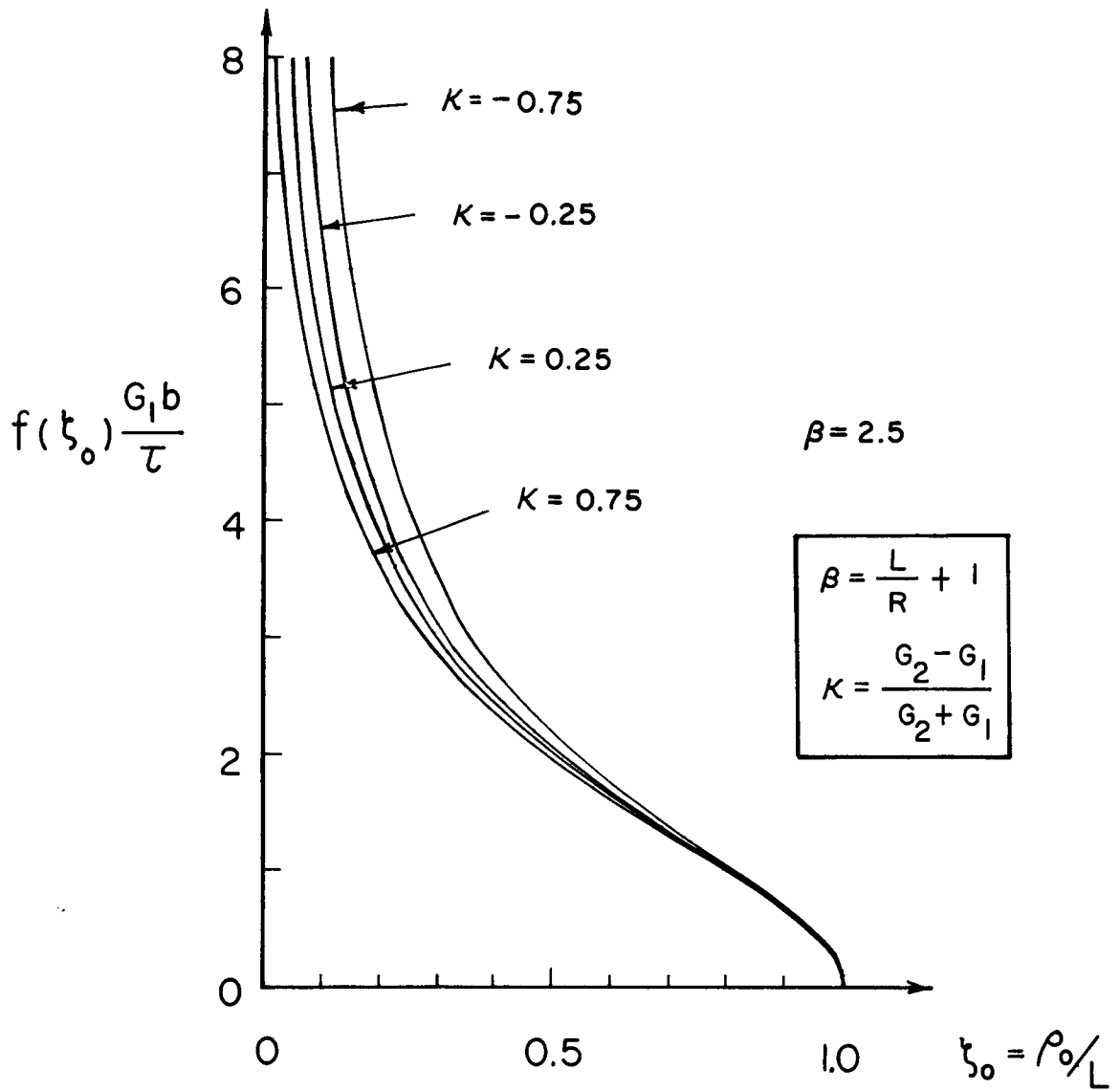


FIGURE 7: $f(\xi_0)$, The Dislocation Distribution Function, vs. ξ_0 for a Fixed L/R Ratio and Various Values of Relative Rigidity (κ).

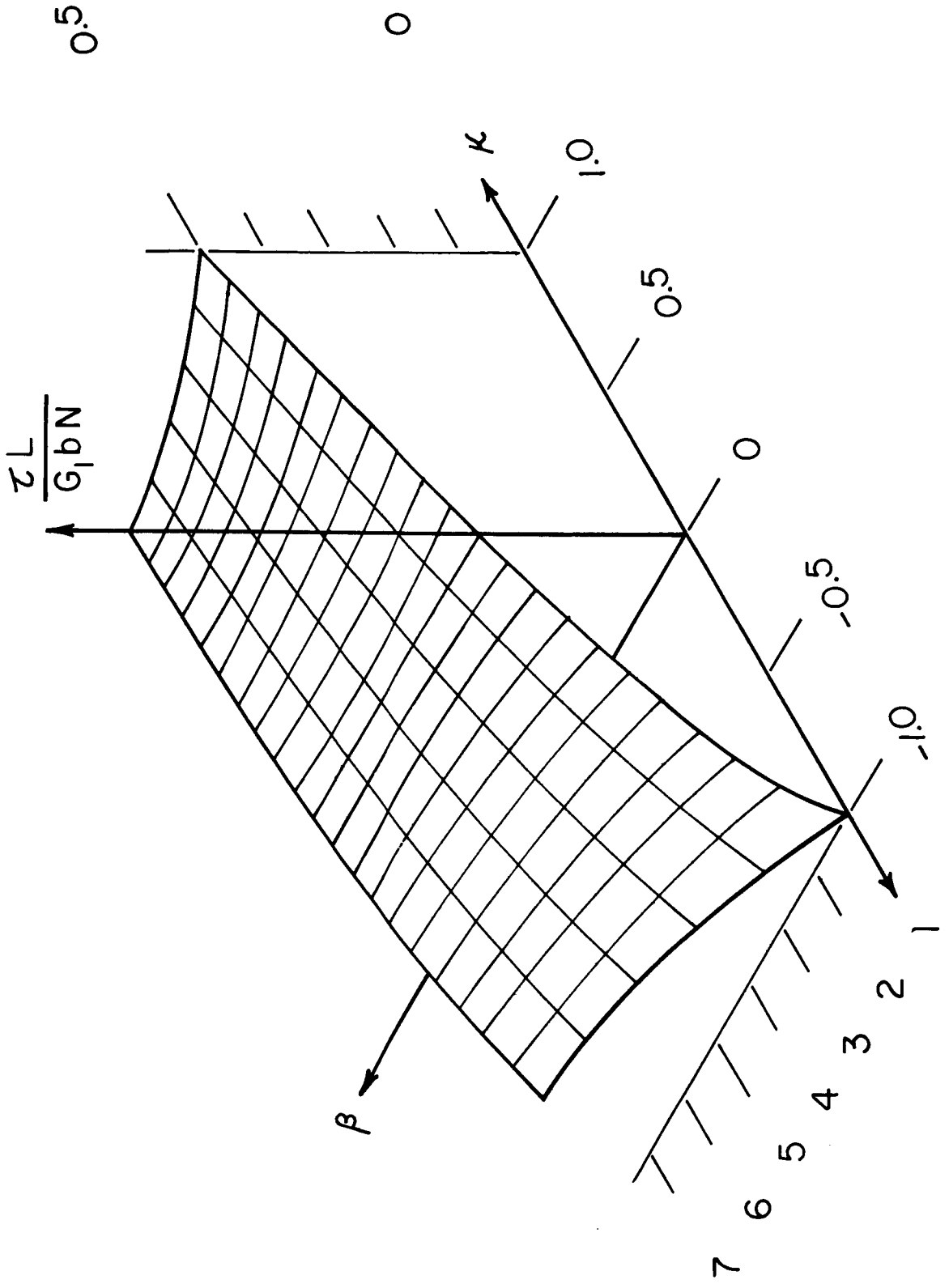


FIGURE 8: The 3-Dimensional Surface $\tau L/G_1 b N$, where N is the Number of Piled-Up Dislocations, as a Function of β and κ .

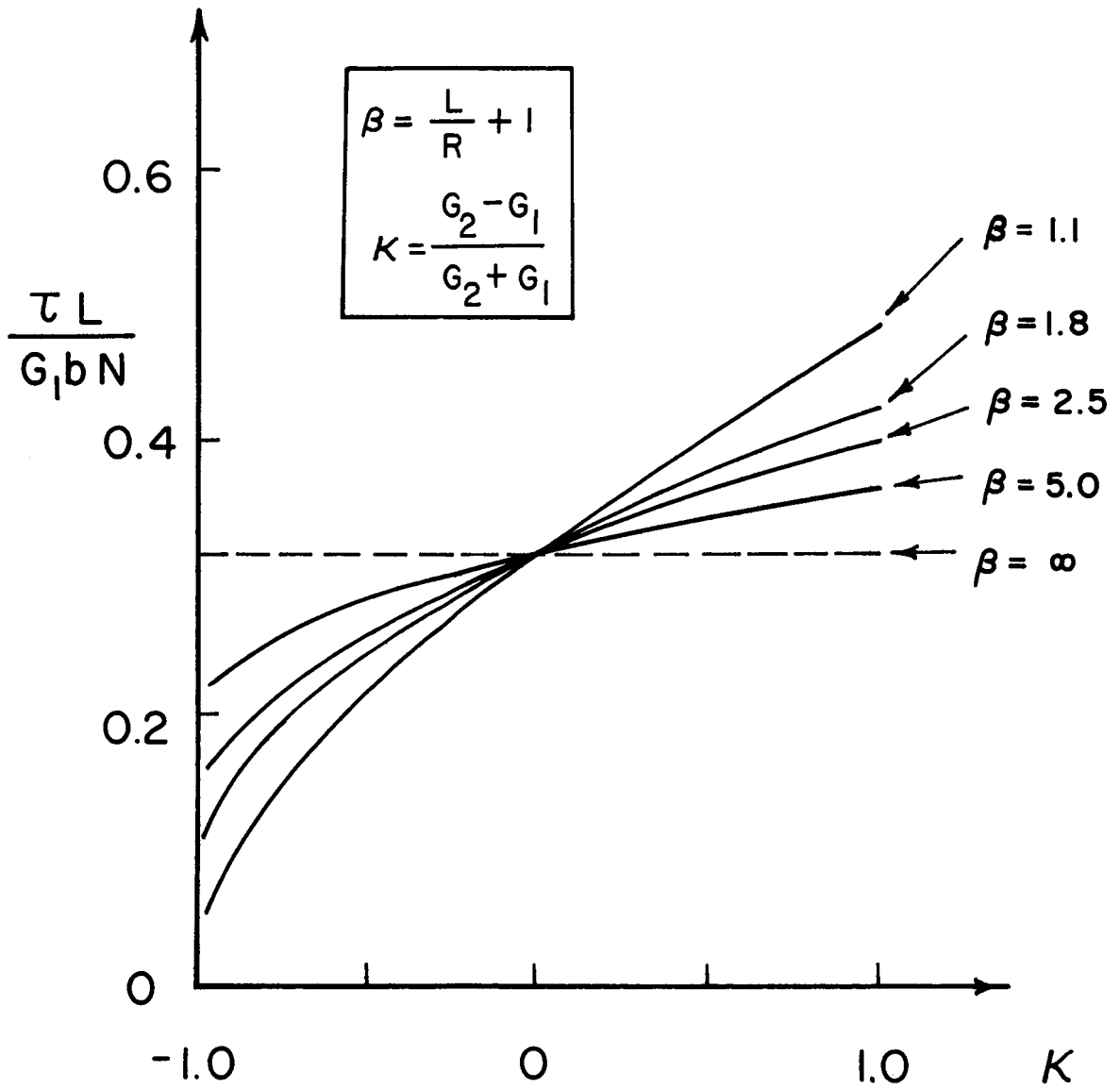


FIGURE 9: $\tau L / G_1 b N$ as a Function of Relative Rigidity (κ) for Various L/R Ratios.

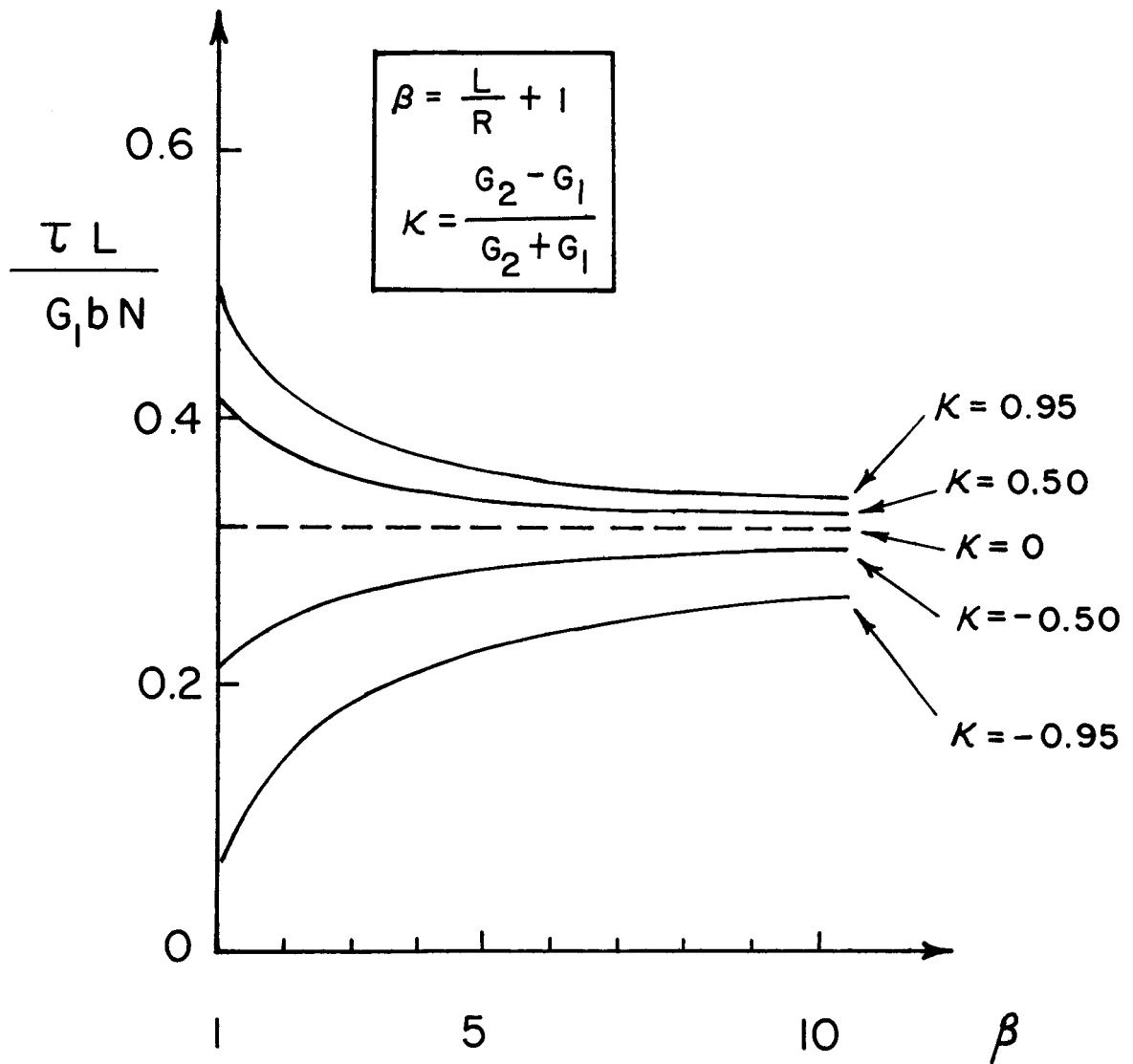


FIGURE 10: $\tau L / G_1 b N$ as a Function of β for Various Values of Relative Rigidity (κ).

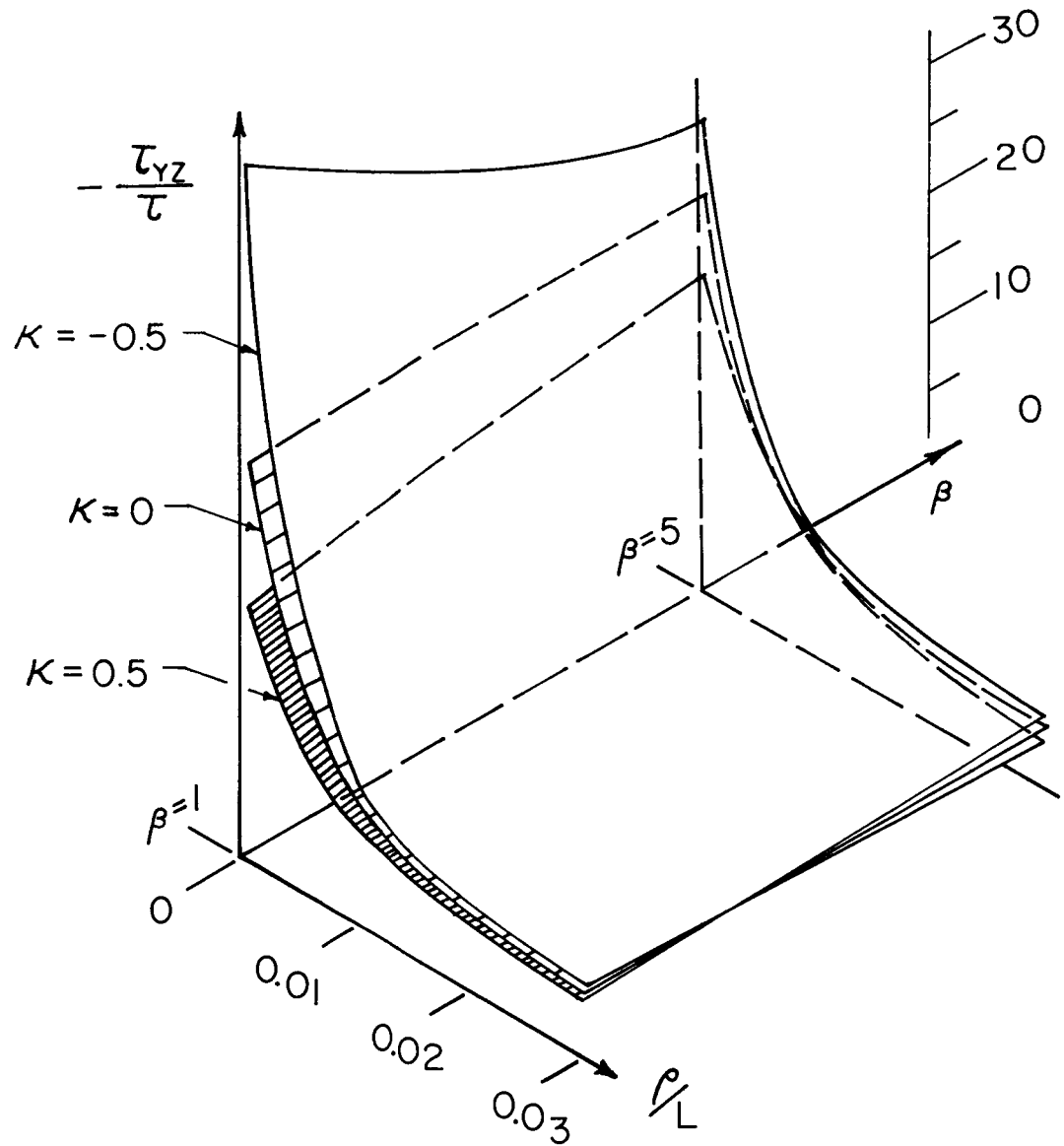


FIGURE 11: Three Dimensional Surfaces Showing the Shear Stress τ_{yz} on the Slip Plane $y = 0$ Inside the Inclusion Close to the Pileup Tip as a Function of β and ρ/L . ρ is the Distance Measured from the Pileup Tip. Each Surface Represents a Different Value of Relative Rigidity (κ).

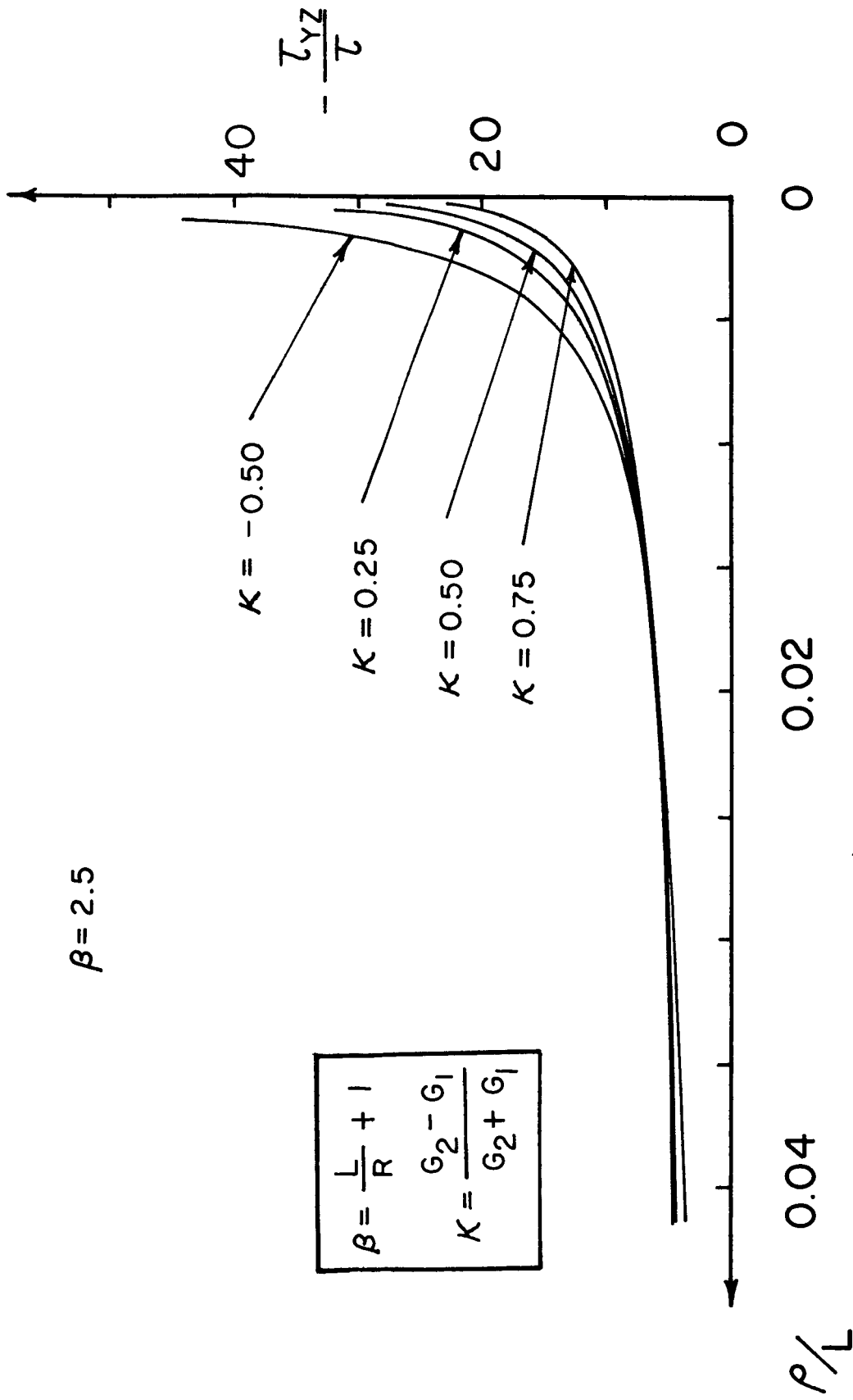


FIGURE 12: τ_{yz} ($y = 0$) Inside the Inclusion Close to the Pileup Tip for a Fixed L/R Ratio and Various Relative Rigidity (K) Values.

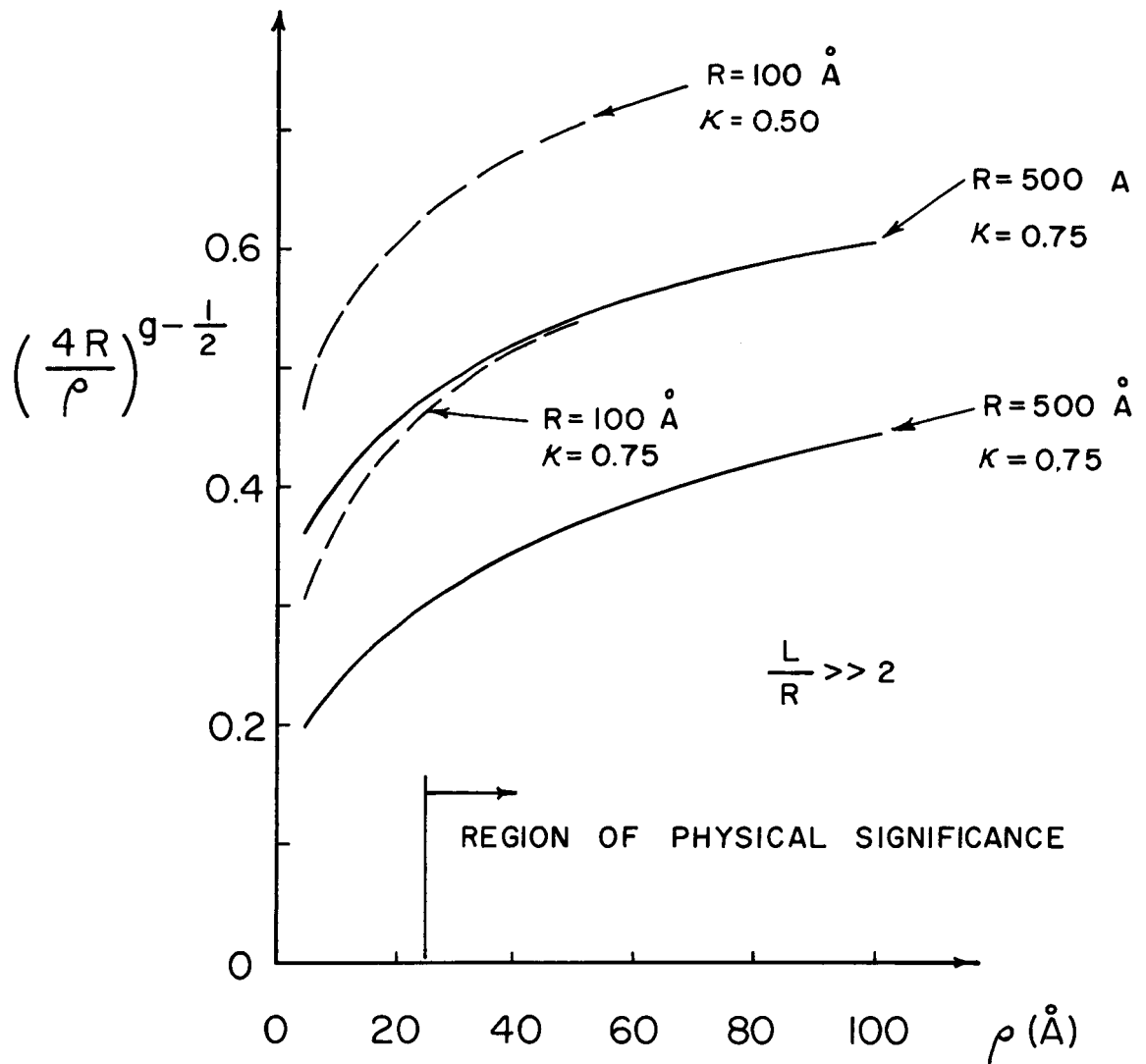


FIGURE 13: The Correction Factor For the Local Stresses in the Second Phase as a Function of ρ for Two Different Size Particles and Two Different Relative Rigidities.

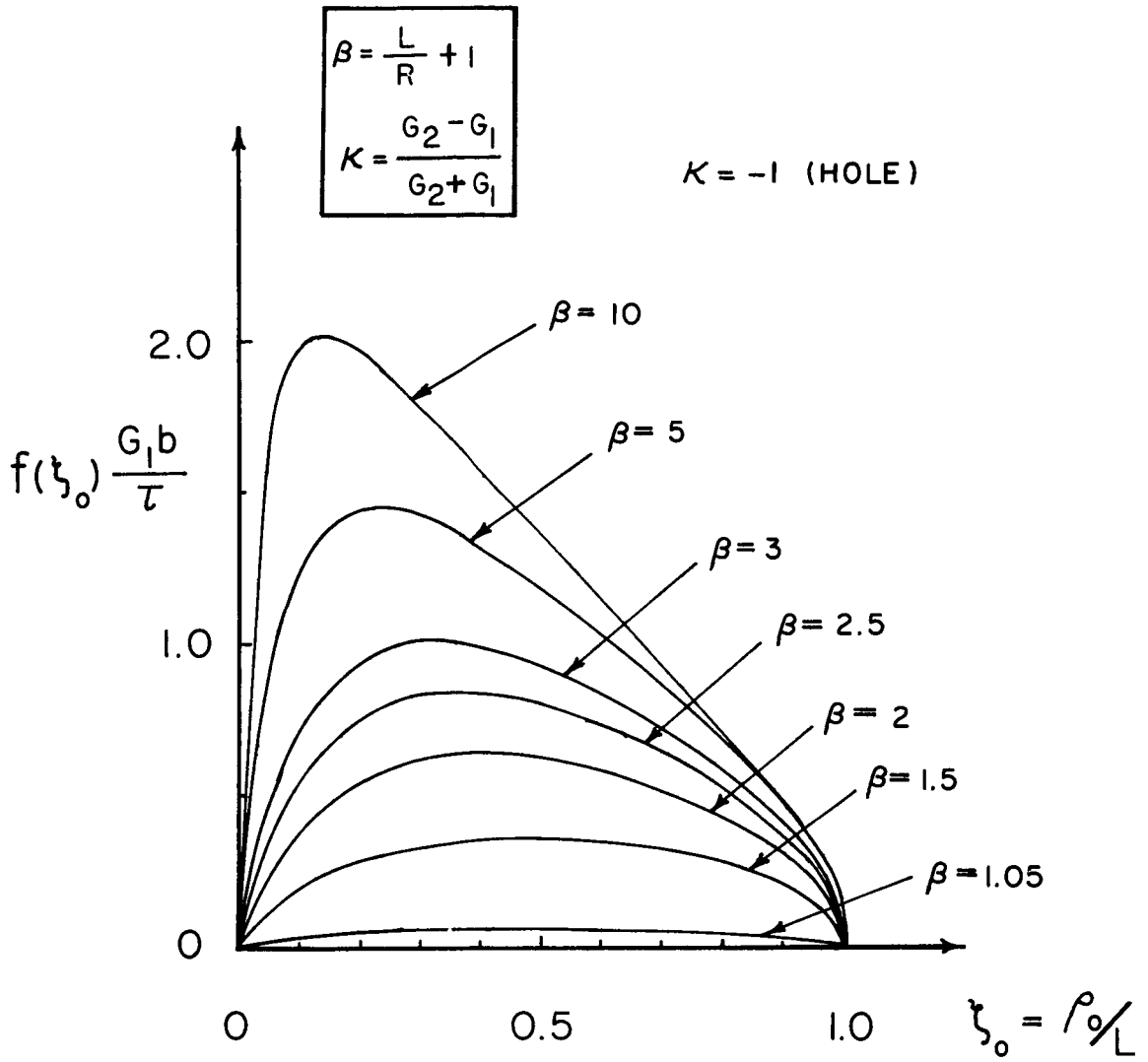


FIGURE 14: $f(\xi_0)$, The Distribution Function for the Hole vs. ξ_0 , for Various Values of L/R .

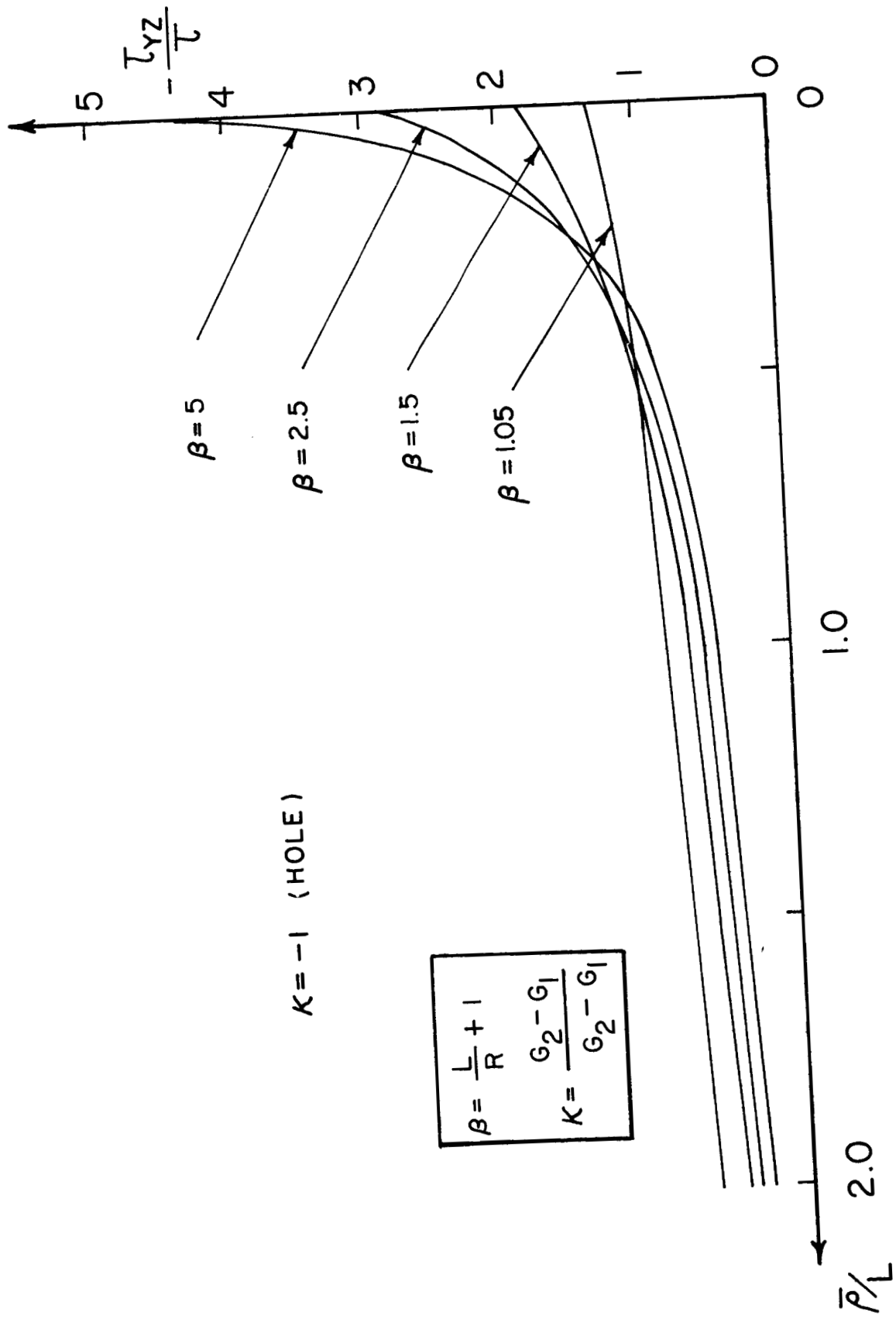


FIGURE 15: The Shear Stress τ_{yz} on the Slip Plane $y = 0$ Outside a Hole. \bar{r} is the Distance Measured Along the Slip Plane from the Point $(-R, 0)$.

APPENDIX

Consider $\oint_C I_1(u, \lambda) du$, where $I_1(u, \lambda)$ is defined by equation (8) in the text, and C is the indented rectangle in the complex $u = v+i\Omega$ plane (Figure 4). If we let $v_0 \rightarrow \infty$, $\epsilon \rightarrow 0$, apply the Cauchy residue theorem, and choose

$$\kappa = \cos g\pi = -\cos w\pi, \quad (A1)$$

then

$$\oint_C I_1(u, \lambda) du = \int_{-\infty}^{\infty} I_1(u, \lambda) du + \kappa \int_{-\infty}^{\infty} I_2(u, \lambda) du \quad (A2)$$

$$= 2\pi i \sum (\text{residues of } I_1(u, \lambda) \text{ at the poles contained inside } C), \quad (A3)$$

where $I_2(u, \lambda)$ is defined by equation (8) in the text. Evaluating the residues of the integrand, equations (A2) and (A3) are equivalent to

$$\begin{aligned} & \int_1^B \frac{f_0(\xi) d\xi}{\lambda - \xi} + \kappa \int_1^B \frac{f_0(\xi) d\xi}{\lambda - \frac{1}{\xi}} \\ &= \left\{ \pi[A \sin g\gamma_0 + B \sin w\gamma_0] + \frac{A \sin g(\pi-\gamma_0) - B \sin w(\pi-\gamma_0)}{\lambda^2} \pi \right. \\ & \quad \left. + \frac{2\pi \cot \gamma_0}{\lambda} [gA \cos g(\pi-\gamma_0) - wB \cos w(\pi-\gamma_0)] \right\}, \quad (A4) \end{aligned}$$

where

$$0 \leq \gamma_0 = \cos^{-1} \frac{\beta-1}{\beta+1} \leq \frac{\pi}{2}, \quad (\text{A5})$$

and $f_0(\xi)$ is defined by equation (6) in the text.

By comparing equation (A4) with equation (4) in the text, we then require

$$\left. \begin{aligned} A \sin g\gamma_0 + B \sin w\gamma_0 &= \frac{2R\tau}{G_1 b} \\ A \sin g(\pi-\gamma_0) - B \sin w(\pi-\gamma_0) &= 0, \end{aligned} \right\} \quad (\text{A6})$$

so that A and B are given by equation (10) in the text.

Thus, $f_0(\xi)$ is a solution to

$$\int_1^\beta \frac{f_0(\xi) d\xi}{\lambda - \xi} + \kappa \int_1^\beta \frac{f_0(\xi) d\xi}{\lambda - \frac{1}{\xi}} = \frac{\kappa N_0}{\lambda} + \frac{2\pi R\tau}{G_1 b} - \frac{\alpha_0}{\lambda}, \quad (\text{A7})$$

where

$$\begin{aligned} N_0 &= \int_1^\beta f_0(\xi) d\xi \\ &= \frac{2\pi \cot \gamma_0}{1 + \kappa} \left\{ gA[\cos g(\pi-\gamma_0) + \cos g\gamma_0] + wB[\cos w\gamma_0 - \cos w(\pi-\gamma_0)] \right\}, \end{aligned} \quad (\text{A8})$$

and

$$\alpha_0 = \frac{\kappa N_0}{\lambda} - 2\pi \cot \gamma_0 [gA \cos g(\pi-\gamma_0) - wB \cos w(\pi-\gamma_0)] \quad (\text{A9})$$

Since $\alpha_0 \neq 0$, the total distribution function must be given by $f_0(\xi) + f_1(\xi)$, where $f_1(\xi)$ is a solution to

$$\int_1^{\beta} \frac{f_1(\xi) d\xi}{\lambda - \xi} + \kappa \int_1^{\beta} \frac{f_1(\xi) d\xi}{\lambda - \frac{1}{\xi}} = \frac{\kappa N_1}{\lambda} + \frac{\alpha_0}{\lambda}, \quad (\text{A10})$$

where

$$N_1 = \int_1^{\beta} f_1(\xi) d\xi.$$

Choosing $f_1(\xi)$ to be given by equation (14) in the text and using the technique described above, the exact solution $f(\xi) = f_0(\xi) + f_1(\xi)$, is found to be given by equation (16) in the text. One should note that equation (A1) is equivalent to

$$g = \frac{2}{\pi} \sin^{-1} \sqrt{\frac{1-\kappa}{2}} = 1 - w. \quad (\text{A11})$$